(SP) (1:100; Zymed, San Francisco, CA), calcitonin gene-related protein (CGRP) (1:2000; Chemicon, Temecula, CA), neurokinin receptor (NK1) (Dr. R. Shigemoto, Kyoto University, Japan), or Fos (1:1000; Santa Cruz Biotechnology, Santa Cruz, CA) for 20 h at 4°C, followed by incubation with biotinylated goat anti-rabbit IgG (Vector Labs, Burlingame, CA; 1:100 in blocking solution) and fluorescein isothiocyanate (FITC) avidin D (1:100; Vector Labs). For Fos immunostaining of the spinal cord, after incubation with an avidin–biotin enzyme complex (Vector Labs; 1:100 in blocking solution) for 90 min at room temperature, immunoreaction was visualized using an ammonium nickel sulfate enhanced diaminobenzidine (DAB) reaction. We counted cells in 7 serial sections of the DRG and 10 sections of the spinal cord. The number of Dan-, SP-, and CGRP-IR neurons in the DRG, and Fos-IR neurons in the laminae I, II, and those in the deep layers (laminae III–VI) were counted.

Double-labeling immunohistochemistry

After incubation with rabbit antibody to Dan for 20 h at 4°C, sections were incubated with goat anti-rabbit Alexa 488 (FITC) (1:400; Molecular Probes Inc., Eugene, OR).

Sections were incubated with mouse antibody to CGRP (marker for peptergic small neurons; 1:2000; Chemicon, Temecula, CA), isolection B4 (IB4; marker for non-peptidergic small neurons; 1:1000; Chemicon, Temecula, CA), guinea pig antibody to P2X3 (marker for non-peptidergic small neurons; 1:2000; Neuromic, Minneapolis, MN), or mouse antibody to neurofilament 200 (NF200; marker for myelinated A fiber s neurons; 1:1000; Chemicon, Temecula, CA) for 20 h at 4°C CGRP, isolectin B4, P2X3 and NF200 were visualized by following incubation with goat anti-mouse Alexa 594 (Texas red; 1:400), streptavidin Alexa 594 (Texas red; 1:400), goat anti-guinea pig Alexa 594 (Texas red; 1:400), and goat anti-mouse Alexa 594 (Texas red; 1:400), respectively.

Statistical analysis

The differences among the groups were compared using ANOVA. Differences were considered to be statistically significant at $P < 0.05$.

Acknowledgments

We thank Dr. R. Shigemoto (Kyoto University) for the gift of antibody to NK1 and K. Kitajo for technical assistance.

References

Abbadie, C., Brown, J.L., Mantyh, P.W., Basbaum, A.I., 1996. Spinal cord substance P receptor immunoreactivity increases in both inflammatory and nerve injury models of persistent pain. Neuroscience 70, 201–209.

Ai, X., Cappuzzello, J., Hall, A.K., 1999. Activin and bone morphogenetic proteins induce calcitonin gene-related peptide in embryonic sensory neurons in vitro. Mol. Cell. Neurosci. 14, 506–518.

Bradbury, E.J., Burnstock, G., McMahon, S.B., 1998. The expression of P2X3 purinoreceptors in sensory neurons: effects of axotomy and glial-derived neurotrophic factor. Mol. Cell. Neurosci. 12, 256–268.

Catheline, G., Le Guen, S., Honore, P., Besson, J.M., 1999. Are there long-term changes in the basal or evoked Fos expression in the dorsal horn of the spinal cord of the mononeuropathic rat? Pain 80, 347–357.

Chaplan, S.R., Bach, F.W., Pogrel, J.W., Chung, J.M., Yaksh, T.L., 1994. Quantitative assessment of tactile allodynia in the rat paw. J. Neurosci. Methods 53, 55–63.

Chi, S.I., Levine, J.D., Basbaum, A.I., 1993. Effects of injury discharge on the persistent expression of spinal cord *fos*-like immunoreactivity produced by sciatic nerve transection in the rat. Brain Res. 617, 220–224.

Dai, Y., Iwata, K., Kondo, E., Morimoto, T., Noguchi, K., 2001. A selective increase in Fos expression in spinal dorsal horn neurons following graded thermal stimulation in rats with experimental mononeuropathy. Pain 90, 287–296.

Dionne, M.S., Skarnes, W.C., Harland, R.M., 2001. Mutation and analysis of Dan, the founding member of the Dan family of transforming growth factor beta antagonists. Mol. Cell. Biol. 21, 636–643.

Donnerer, J., Schuligo, I.R., Stein, C., 1992. Increased content and transport of substance P and calcitonin gene-related peptide in sensory nerves innervating inflamed tissue: evidence for a regulatory function of nerve growth factor in vivo. Neuroscience 49, 693–698.

Hargreaves, K., Dubner, R., Brown, F., Flores, C., Joris, J., 1988. A new and sensitive method for measuring thermal nociception in cutaneous hyperalgesia. Pain 32, 77–88.

Hudspith, M.J., Harrisson, S., Smith, G., Bountra, C., Elliot, P.J., Birch, P.J., Hunt, S.P., Munglani, R., 1999. Effect of post-injury NMDA antagonist treatment on long-term *fos* expression and hyperalgesia in a model of chronic neuropathic pain. Brain Res. 822, 220–227.

Hsu, D.R., Economides, A.N., Wang, X., Eimon, P.M., Harland, R.M., 1998. The *Xenopus* dorsalizing factor Gremlin identifies a novel family of secreted proteins that antagonize BMP activities. Mol. Cell 1, 673–683.

Hunt, S.P., Pini, A., Evan, G., 1987. Induction of c-*fos*-like protein in spinal cord neurons following sensory stimulation. Nature 328, 632–634.

Liu, T., Tracey, D.J., 2000. ATP P2X receptors play little role in the maintenance of neuropathic hyperalgesia. NeuroReport 11, 1669–1672.

Llewellyn-Smith, I.J., Burnstock, G., 1998. Ultrastructural localization of P2X3 receptors in rat sensory neurons. NeuroReport 9, 2545–2550.

Ma, Q.P., Woolf, C.J., 1996. Basal and touch-evoked *fos*-like immunoreactivity during experimental inflammation in the rat. Pain 67, 307–316.

Malmberg, A.B., Chen, C., Tonegawa, S., Basbaum, A.I., 1997. Preserved acute pain and reduced neuropathic pain in mice lacking PKCgamma. Science 278, 279–283.

McCarson, K., Krause, J.E., 1994. NK-1 and NK-3 type tachykinin receptor mRNA expression in the rat spinal cord dorsal horn is increased during adjuvant or formalin induced nociception. J. Neurosci. 14, 712–720.

Neumann, S., Doubell, T.P., Leslie, T., Woolf, C.J., 1996. Inflammatory pain hypersensitivity mediated by phenotypic switch in myelinated primary sensory neurons. Nature 384, 360–364.

Noguchi, K., Ruda, M.A., 1992. Gene regulation in an ascending nociceptive pathway: inflammation-induced increase in preprotachykinin mRNA in rat lamina I spinal projection neurons. J. Neurosci. 12, 2563–2572.

Noguchi, K., Kawai, Y., Fukuoka, T., Senba, E., Miki, K., 1995. Substance P induced by peripheral nerve injury in primary afferent sensory neurons and its effect on dorsal column nucleus neurons. J. Neurosci. 11, 7633–7643.

Noguchi, K., Morita, Y., Kiyama, H., Ono, K., Tohyama, M., 1988. A noxious stimulus induces the preprotachykinin-A gene expression in the rat dorsal root ganglion: a quantitative study using in situ hybridization histochemistry. Brain Res. 464, 31–35.

Ohtori, S., Yamamoto, T., Ino, H., Hanaoka, E., Shinbo, J., Ozaki, T., Takada, N., Nakamura, Y., Chiba, T., Nakagawara, A., Sakiyama, S., Sakashita, Y., Takahashi, K., Tanaka, K., Yamagata, M., Yamazaki, M., Shimizu, S., Moriya, H., 2002. Differential screening-selected gene aberrative in neuroblastoma protein modulates inflammatory pain in the spinal dorsal horn. Neuroscience 110, 579–586.

Ozaki, T., Sakiyama, S., 1993. Molecular cloning and characterization of a cDNA showing negative regulation in v-*src*-transformed 3Y1 rat fibroblasts. Proc. Natl. Acad. Sci. U. S. A. 90, 2593–2597.

Ozaki, T., Sakiyama, S., 1994. Tumor-suppressive activity of N03 gene product in v-*src*-transformed rat 3Y1 fibroblasts. Cancer Res. 54, 646–648.

Ozaki, T., Nakamura, Y., Enomoto, H., HilRose, M., Sakiyama, S., 1995. Overexpression of DAN gene product in normal rat fibroblasts causes a retardation of the entry into the S phase. Cancer Res. 55, 895–900.

Pearce, J.J., Penny, G., Rossant, J., 1999. A mouse cerberus/Dan-related gene family. Dev. Biol. 209, 98–110.

Piccolo, S., Agius, E., Leyns, L., Bhattacharyya, S., Grunz, H., Bouwmeester, T., De Robertis, E.M., 1999. The head inducer Cerberus is a multifunctional antagonist of Nodal. BMP and Wnt signals. Nature 397, 707–710.

Schaible, H.G., Freudenberger, U., Neugebauer, V., Stiller, R.U., 1994. Intraspinal release of immunoreactive calcitonin gene-related peptide during development of inflammation in the joint in vivo-a study with antibody microprobes in cat and rat. Neuroscience 62, 1293–1305.

Sivilotti, L., Woolf, C.J., 1994. The contribution of GABAA and glycine receptors to central sensitization: disinhibition and touch-evoked allodynia in the spinal cord. J. Neurophysiol. 72, 169–179.

Stanfa, L.C., Kontinen, V.K., Dickenson, A.H., 2000. Effects of spinally administered P2X receptor agonists and antagonists on the responses of dorsal horn neurones recorded in normal, carrageenan-inflamed and neuropathic rats. Br. J. Pharmacol. 129, 351–359.

Stanley, E., Biben, C., Kotecha, S., Fabri, L., Tajbakhsh, S., Wang, C.C., Hatzistavrou, T., Roberts, B., Drinkwater, C., Lah, M., Buckingham, M., Hilton, D., Nash, A., Mohun, T., Harvey, R.P., 1998. DAN is a secreted glycoprotein related to *Xenopus* cerberus. Mech. Dev. 77, 173–184.

Todd, A.J., Puskar, Z., Spike, R.C., Hughes, C., Watt, C., Forrest, L., 2002. Projection neurons in lamina I of rat spinal cord with the neurokinin 1 receptor are selectively innervated by substance P-containing afferents and respond to noxious stimulation. J. Neurosci. 22, 4103–4113.

Identification of novel human neuronal leucine-rich repeat (h*NLRR*) family genes and inverse association of expression of *Nbla10449/*h*NLRR-1* and *Nbla10677/*h*NLRR-3* with the prognosis of primary neuroblastomas

SHIHO HAMANO[1,2], MIKI OHIRA[1], ERIKO ISOGAI[1], KOUNOSUKE NAKADA[2] and AKIRA NAKAGAWARA[1]

[1]Division of Biochemistry, Chiba Cancer Center Research Institute, 666-2 Nitona, Chuoh-ku, Chiba 260-8717; [2]Division of Pediatric Surgery, St. Marianna University School of Medicine, 2-16-1 Sugao, Miyamae-ku, Kawasaki 216-8511, Japan

Received August 1, 2003; Accepted September 24, 2003

Abstract. To search for novel prognostic indicators, we previously cloned >2,000 novel genes from primary neuroblastoma (NBL) cDNA libraries and screened for differential expression between the subsets with favorable (stage 1 or 2 with a single copy of *MYCN*) and unfavorable (stage 3 or 4 with amplification of *MYCN*) prognosis. From them, we have identified 3 genes of human neuronal leucine-rich repeat protein (NLRR) family: *Nbla10449/*h*NLRR-1*, *Nbla00061/*h*NLRR-2/GAC1* and *Nbla10677/*h*NLRR-3*. An additional family member, h*NLRR-5*, was also found by homology search against public database. NLRR family proteins have been proposed to function as a neuronal adhesion molecule or soluble ligand binding receptor like *Drosophila toll* and *slit* with multiple domains including 11 sets of extracellular leucine-rich repeat (LRR)-motifs. However, the functional role of the NLRR protein family has been elusive. Our present study shows that h*NLRR* mRNAs are preferentially expressed in nervous system and/or adrenal gland. In cancer cell lines, h*NLRR-1*, h*NLRR-3* and h*NLRR-5* are expressed at high levels in the neural crest-derived cells. Most remarkably, in primary NBLs, h*NLRR-1* is significantly expressed at high levels in unfavorable subsets as compared to favorable ones, whereas the expression pattern of h*NLRR-3* and h*NLRR-5* is the opposite. In order to understand the function of these receptors, we have used newborn mouse superior cervical ganglion (SCG) cells which are dependent on nerve growth factor (NGF) for their survival. Expression of the mouse counterparts of h*NLRR-2* and h*NLRR-3* is up-regulated after NGF-induced differentiation and down-regulated after NGF depletion-induced apoptosis. On the other hand, expression of h*NLRR-1* and h*NLRR-5* is inversely regulated in the same system. These results have suggested that the regulation of the h*NLRR* family genes may be associated with NGF signaling pathway in both SCG cells and neuroblastoma. Our quantitative real-time RT-PCR analysis using 99 primary NBLs has revealed that high levels of h*NLRR-1* expression are significantly associated with older age (>1 year, p=0.0001), advanced stages (p=0.0007), low expression of *TrkA* (p=0.011), and *MYCN* amplification (p=0.0001), while those of h*NLRR-3* expression are significantly correlated with the favorable prognostic indicators. Furthermore, multivariate analysis reveals that expression of h*NLRR-1* is an independent prognostic indicator in human neuroblastoma. Thus, our results demonstrate that, despite being members of the same family, h*NLRR-1* and h*NLRR-3* may share different biological function among the NBL subsets, and that their expression level becomes novel prognostic indicators of NBL.

Introduction

Neuroblastoma (NBL) is one of the most common pediatric tumors originating from sympathoadrenal lineage of the neural crest. NBL shows variable biological behavior which characterizes different clinical subsets (1). The tumors found in young children, <1 year of age usually regress spontaneously, while those in the older children are often aggressive leading to poor outcome. Recent advances in molecular biology have identified the important molecules involved in the regulation of growth, differentiation and programmed cell death during development of the sympathoadrenal cells (2), some of which link to the modulation of NBL biology. These include Trk family tyrosine kinase receptors and *MYCN* proto-oncogene. TrkA, a high-affinity receptor for nerve growth factor (NGF), is expressed in favorable subsets of NBL and regulates differentiation and/or regression of the tumor cells (3). On the other hand, TrkB, a receptor for brain-derived neurotrophic factor (BDNF) and neurotrophin-4 (NT-4), is expressed in NBLs with unfavorable prognosis. An autocrine loop of BDNF/NT-4 and TrkB may promote tumor cell survival and increase their invasiveness (4). Amplification of *MYCN* is significantly associated with allelic loss of the

Correspondence to: Dr Akira Nakagawara, Division of Biochemistry, Chiba Cancer Center Research Institute, 666-2 Nitona, Chuoh-ku, Chiba 260-8717, Japan
E-mail: akiranak@chiba-ccri.chuo.chiba.jp

Key words: leucine-rich repeat, neuroblastoma, differential expression, prognostic factor

distal region of chromosome 1, and both are indicators of poor prognosis. A recent report suggests that *MYCN* oncoprotein induces expression of *Id-2* with a helix-loop-helix domain and in turn negatively regulates Rb tumor suppressor in NBL (5). However, many important genes may still be missing for better understanding of NBL biology as well as predicting the prognosis. In order to identify novel NBL-related genes and promote better understanding of the molecular mechanism of NBL genesis and its biology, differential screening method has been applied (6).

We have previously constructed full-length-enriched oligocapping cDNA libraries from different subsets of primary NBL (6,7). One derived from the mixture of favorable NBLs in stage 1 with single-copy of *MYCN*, and the other from unfavorable NBLs in stage 3 and 4 with *MYCN* amplification. We have finished end-sequencing of 2,500 clones obtained from each library, and found that the expression profile is markedly different between the subsets. So far, 1,800 independent genes from these libraries have been subjected to semi-quantitative RT-PCR using 16 favorable and 16 unfavorable NBLs to find the genes differentially expressed between favorable (F) and unfavorable (UF) subsets (8,9).

In this study, we have identified novel human *NLRR* family genes that are differentially expressed among the NBL subsets. NLRRs are proteins with leucine-rich repeat (LRR) domains which may be involved in protein-protein interactions (10). They may also function as cell-adhesion molecules or signaling receptors implicated in regulation of the neural development. Expression of the h*NLRR-1/Nbla10449* gene is significantly associated with short survival as well as conventional poor-prognostic factors, whereas that of the h*NLRR-3/Nbla10677* gene is increased in favorable subset of NBL. Our results suggest that the differential expression of h*NLRR* genes among the NBL subsets is involved in the regulation of growth, differentiation and cell death of human NBL.

Materials and methods

Patients. We studied tumors from 99 children with NBL diagnosed between 1995-1999. Fifty-four Japanese patients were identified by a mass screening program started in 1985 (9,10). The selection of tumors for this study was solely based on the availability of a sufficient amount of tumor tissue, from which DNA and mRNA could be prepared for the analyses described below.

The diagnosis of NBL was confirmed by histologic assessment of the tumor specimen obtained at surgery according to the classification of Shimada *et al* (11). There were 57 tumors with favorable histology, and 42 with unfavorable histology. The tumors were staged according to the International Neuroblastoma Staging System (INSS) (12). Thirty-eight tumors (36 identified by mass screening) were stage 1, 14 (11 identified by mass screening) stage 2, 5 (3 identified by mass screening) stage 4s, 10 (3 identified by mass screening) stage 3, and 32 (1 identified by mass screening) stage 4. The patients were treated according to the protocols previously described (13).

Tumor samples and cell lines. Fresh, frozen tumorous tissues were sent to the Division of Biochemistry, Chiba Cancer Center Research Institute, from various hospitals in Japan with informed consent from the patient's parents. All samples were obtained by surgery (or biopsy) and stored at -80˚C. Studies were approved by the Institutional Review Board of the Chiba Cancer Center. Human cell lines which we used included NBL (CHP134, CHP901, GANB, GOTO, IMR32, SMS-KAN, SMS-KCN, KP-N-NS, LAN-5, NB-1, NB-9, NBKM-1, NB (Tu)-1, NLF, NMB, RTBM1, SMS-SAN, SK-N-BE, SK-N-DZ, TNB, TGW, LHN, NGP, NB69, NBL-S, OAN, SK-N-AS, SK-N-SH, SH-SY5Y, and CNB-RT), osteosarcoma (OST, Saos2, and NOS1), rhabdomyosarcoma (RMS-MK and ASPS-KY), colorectal adenocarcinoma (COLO320, SW480, and LOVO), a hepatocellular cancer (HepG2), breast cancer (MOA-MB-453 and MB231), melanoma (G361, G32TG, A875), a thyroid cancer (TTC11), a gastric cancer (KATO3), esophageal cancer (ECGI10), a pancreatic cancer (ASPC1) and a lung cancer cell lines (A549). The cells were cultured in the RPMI-1640 medium (Nissui Pharmaceutical Co. Ltd., Tokyo) with 10% fetal bovine serum and 50 µg/ml penicillin/streptomycin at humidified 5% CO_2/95% air at 37˚C.

Primary culture of newborn mouse superior cervical ganglion cells. The SCG neurons were isolated from newborn mice, and treated with 50 ng/ml of NGF for 5 days, as previously reported (14). RNAs were isolated 12, 24, and 48 h after depleting NGF and adding anti-NGF antibody (1% v/v).

Northern blot analysis. Multiple Tissue Northern blot purchased from Clontech (Palo Alto, CA, USA) was used for Northern analysis with cDNA fragments labeled with α-[^{32}P]dCTP as probes. Hybridization was performed in the ExpressHyb hybridization buffer (Clontech) at 68˚C for 1 h. Membrane was washed twice in 2X SSC/0.05% SDS at room temperature for 30 min, twice in 0.1X SSC/0.1% SDS at 50˚C for 40 min. After washing, the filter was autoradiographed with X-ray film. The membrane was boiled in 0.1% SDS for 10 min for reprobing, and rehybridized with ß-actin as a control.

Semi-quantitative RT-PCR. cDNA was synthesized from 5 µg of total RNA in a 20 µl reaction mixture containing 200 units of Superscript II reverse transcriptase (Life Technologies, Inc.) and pd(N)$_6$ random hexamer (Takara Shuzo Co., Ltd., Ohtsu, Japan). The resulting cDNA fragments were diluted to be a 1:10 solution for PCR templates. The following pairs of forward and reverse primer sets were prepared for amplification: *NLRR-1*, 5'-GTCGATGTCCATGAATACAACCT-3' and 5'-CAAGGCTAATGACGGCAAAC-3'; *NLRR-2*, 5'-TGACCTATTCCTGACGG-3' and 5'-AAATCACAGTCTCGGGC-3'; *NLRR-3*, 5'-ACTCTTGCCTAATACCCTGAC-3' and 5'-AGATGGTATTCGAGCACTTTG-3'; *GAPDH*, 5'-CTGCACCAACAATATCCC-3' and 5'-GTAGAGACAGGGTTTCAC-3'. All PCR amplifications were performed with a Perkin-Elmer Corp. GeneAmp PCR 9700, using rTaq polymerase (Takara Shuzo Co., Ltd.) with 35 cycles of sequential denaturation (95˚C for 15 sec) and annealing-extension (58˚C for 15 sec and 72˚C for 1 min). *GAPDH* was used as a control and amplified under the same condition except for reduced amplification cycles to 28. PCR templates

were standardized by its *GAPDH* expression before performing semi-quantitative PCR. The products were electrophoresed on 2.0% agarose gels and stained with ethdium bromide for visualization.

Quantitative real-time RT-PCR. cDNA was prepared by the same method as in the semi-quantitative RT-PCR and 2 µl of the 40-fold dilution was used for each PCR reaction. Primers and TaqMan probes for *Nbla10449* and *Nbla10677* were designed using the primer design software Primer Express™ (Perkin-Elmer Applied Biosystems). TaqMan GAPDH control reagent kit (Perkin-Elmer Applied Biosystems) was used for *GAPDH* expression as a control. Reaction mixture (25 µl), containing 2 µl of cDNA, 1X TaqMan mixture, 0.3 µM forward and reverse primers, and 0.2 µM TaqMan probe were used for PCR. The condition of PCR was as follows: 2 min at 50°C (stage 1), 10 min at 95°C (stage 2), and then 50 cycles of amplification for 15 sec at 95°C and 1 min at 60°C (stage 3).

Statistical analysis. The student's t-tests were used to explore possible associations between *Nbla10449/hNLRR-1* expression and other factors, such as age. Since the values of the *Nbla10449/hNLRR-1* and *Nbla10677/hNLRR-3* expression were skewed, a log transformation was used to achieve the normality when using t-test and Cox regression. The distinction between high and low levels of *Nbla10449* was based on the median value (low, *Nbla10449* <0.31 d.u.; high, Nbla10449 >0.31 d.u.), regardless of tumor stage, *MYCN* copy number, or survival. The distinction between high and low levels of *Nbla10677* was based on the median value (low, *Nbla10677* <1.04 d.u.; high, *Nbla10677*>1.04 d.u.), regardless of tumor stage, *MYCN* copy number, or survival. Kaplan-Meier survival curves were calculated, and survival distributions were compared using the log-rank test. Cox regression models were used to explore associations between *Nbla10449/Nbla10677*, age, *MYCN* copy number, mass screening, tumor origin and survival. Statistical significance was declared if the p value was <0.05. Statistical analysis was performed using Stata 6.0. (Stata Statistical Software: Release 6.0 College Station, Stata Corporation, TX, 1999).

Results

Identification of novel human homologues of NLRR family genes, Nbla10449/hNLRR-1 and Nbla10677/hNLRR-3, and their differential expression between favorable and unfavorable subsets of neuroblastoma. To identify the genes differentially expressed between favorable and unfavorable NBLs, semi-quantitative RT-PCR analyses were performed. Sixteen favorable (F) and 16 unfavorable (UF) NBLs were used as PCR templates after normalization by GAPDH expression. So far, ~1,800 independent genes from the NBL cDNA libraries have been surveyed, resulting in the approximately 300 genes with differential expression between the subsets (8,9). Among them, we found *Nbla10449* and *Nbla10677* genes that are highly homologous to the mouse *NLRR-1* and *NLRR-3* genes, respectively. *Nbla10449/hNLRR-1* was preferentially expressed in UF NBLs, whereas *Nbla10677/hNLRR-3* was highly expressed in F NBLs (Fig. 3A).

Full-length cDNA cloning and structure of human NLRR-1, NLRR-2, NLRR-3 and NLRR-5 genes. We performed sequencing of whole inserts of *Nbla10449* and *Nbla10677* and defined their full-length cDNA sequences. In addition, during the process, we also identified human *NLRR-5* by homology search on the database. Furthermore, the other clone, *Nbla00061*, was found to be the same gene as *GAC1* which we renamed as h*NLRR-2*. *NLRR-4* has recently been reported by another group (15).

Nbla10449/hNLRR-1. A full-length *Nbla10449* genes comprised 3,060 bp, with an open reading frame (ORF) of 2,151 bp. The deduced protein was 716 a.a. in length, and included 2 hydrophobic stretches corresponding to a signal peptide at the extreme N-terminal region and a deduced transmembrane domain close to the C-terminal region (Fig. 1A). Analysis of the extracellular domain revealed the presence of 11 leucine-rich repeats encompassed by flanking cystein cluster, a leucine-rich repeat N-terminal domain (LRRNT) and a leucine-rich repeat C-terminal domain (LRRCT), a single immunogloblin C2 type domain, and a fibronectin type III domain (Fig. 1). Homology search against public database showed that *Nbla10449* was identical to the human *EST KIAA1497* (GenBank/DDBJ accession number AB040930) which lacked the N-terminal region and was similar to 2 leucine-rich repeat proteins, m*NLRR-1* (acc. no. D45913) and *Xenopus* x*NLRR-1* (acc. no. AB014462). The identities of deduced Nbla10449 protein to mNLRR-1 and xNLRR-1 were 92 and 75%, respectively. We also analyzed genomic structure of *Nbla10449*, and found that this gene comprised of single exon without any intron and mapped to chromosome 3p region.

Nbla10677/hNLRR-3. Nbla10677 comprised 2,471 bp with an ORF of 2,127bp (acc. no. AB060967) without intron, and mapped to chromosome 7q31. The deduced protein contained 708 a.a. and had a similar structure to Nbla10449/hNLRR-1 (Fig. 1A). In addition, the RGD sequence, an integrin-binding domain, was found in the leucine-rich repeats. Homology search showed that *Nbla10677* was identical to human cDNA FLJ11129 (acc. no. AK001991) and highly similar to the leucine-rich repeat proteins of mouse (mNLRR-3; acc. no. D49802) and rat (rNLRR-3; acc. no. AF291437). Therefore, Nbla10677 seemed to be a human NLRR-3. The Nbla10677/hNLRR-3 showed 85 and 83% similarity to mNLRR-3 and rNLRR-3 proteins, respectively.

Nbla00061/GAC1/hNLRR-2. The *Nbla00061* cDNA clone comprised 3,206 bp including a partial ORF of 2,142 bp. Sequence analysis revealed that it is identical to a *glioma amplified on chromosome 1* gene, *GAC1* (acc. no. AF030435), mapped to chromosome 1q32.1. The GAC1 protein, which was previously reported to be a member of an NLRR protein family (15), had 713 a.a. with a similar structure to NLRR-1 and 3 (Fig. 1). GAC1 showed 98% identity to mNLRR-2, although the latter was reported as only a partial sequence (16). It showed only 54 and 50% identities to mNLRR-1 and mNLRR-3, respectively, indicating that Nbla00061/GAC1 is a human counterpart of mNLRR-2.

m*NLRR-4* was cloned by another group from hemangioblast-like cell line derived from E11.5 mouse AGM and its predicted protein has 4 LRRs, fibronectin 3 and EGF-like motives in the extracellular region (Rump A *et al*, The Molecular Biology Society of Japan Conference, Yokohama,

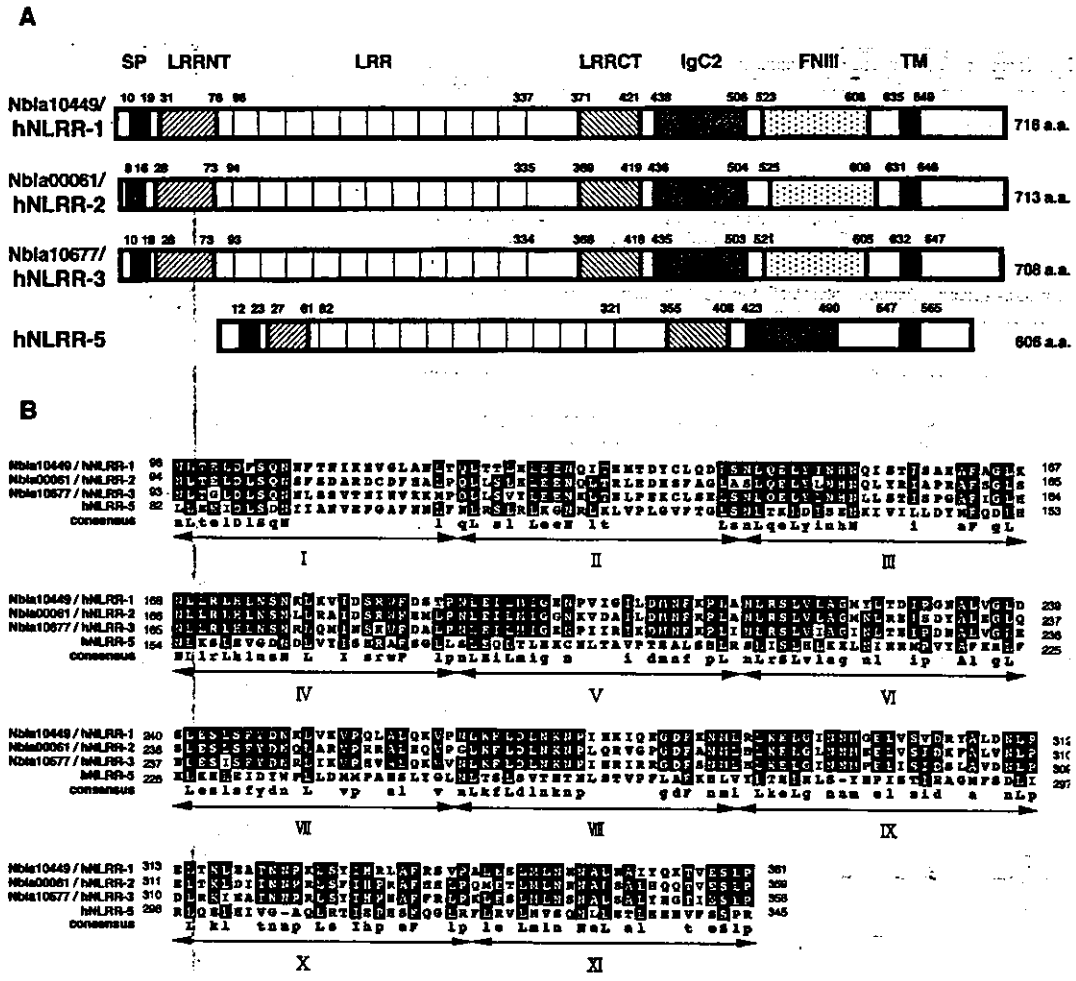

Figure 1. Structures and deduced amino acid sequences of hNLRR families. A, Schematic representation of hNLRR-1, hNLRR-2, hNLRR-3 and hNLRR-5 whose proteins consist of 716, 713, 708 and 606 a.a., respectively. SP, predicted signal peptide; TM, predicted transmembrane region; LRRNT, leucine-rich repeat N-terminal domain; LRRCT, leucine-rich repeat C-terminal domain; LRR, leucine-rich repeat; Igc2, immunoglobulin C-2 type domain; FN III, fibronectin type III domain. B, Amino acid alignment of the LRR domains of hNLRR families. Eleven repeats of LRR motif are shown by Roman numerals. Consensus sequences are highlighted and shown below.

abs. 4P-500 and 4P-501, 2001). h*NLRR-5* has no EGF-like motif and has 11 LRRs, and we failed to identify its human counterpart in the database or our NBL cDNA libraries.

h*NLRR-5*. Homology search against proteins deduced from genomic sequences on chromosome 9p revealed the presence of another family member of NLRR (acc. no. CAC22713). Its deduced protein was 606 a.a. in length and had a similar structure to the other NLRR members. However, a fibronectin domain was not included in this product. It showed 56 and 53% identities to mouse hypothetical protein (acc. no. BAB32403) and *Macaca fascicularis* hypothetical protein (acc. no. BAB03557), respectively, suggesting that they were mouse and *Macaca fascicularis* counterparts of hNLRR-5.

Expression of hNLRR family genes in human tissues. To examine whether *hNLRR* genes display neuron-specific expression, Northern analysis and semi-quantitative RT-PCR were performed. Among several human fetal tissues, h*NLRR-1*, h*NLRR-2* and h*NLRR-3* mRNAs were strongly expressed in brain at the size of 4.0-4.5 kb (Fig. 2A). By contrast, h*NLRR-5* was ubiquitously expressed in all main fetal organs. The size of h*NLRR-2* transcript in the liver was smaller than that in the other tissues. In adult human tissues, all h*NLRR-1*, h*NLRR-2*, h*NLRR-3* and h*NLRR-5* were also preferentially expressed at high levels in the nerve tissues (Fig. 2B).

Expression of hNLRR family genes in neuroblastoma and cell lines. Expression of h*NLRR* family genes was measured in primary neuroblastomas and cell lines using semi-quantitative RT-PCR. As shown in Fig 3A, *Nbla10449/*h*NLRR-1* was highly expressed in UF NBLs, whereas *Nbla10677/*h*NLRR-3* and h*NLRR-5* were preferentially expressed in the F NBLs. *Nbla00061/*h*NLRR-2* seemed to be equally expressed between both subsets. In NBL cell lines, expression of *NLRR-1* was observed relatively more frequently in the lines with *MYCN* amplification than in those with a single copy of the gene. On the other hand, *NLRR-3* appeared to be expressed rather frequently in the cell lines without *MYCN* amplification. Interestingly, however, there was a tendency that the cells with high expression of *NLRR-1* also had a high levels of expression of *NLRR-3* (Fig. 3B). The expression of both h*NLRR-2* and h*NLRR-5* was found in most NBL cell lines.

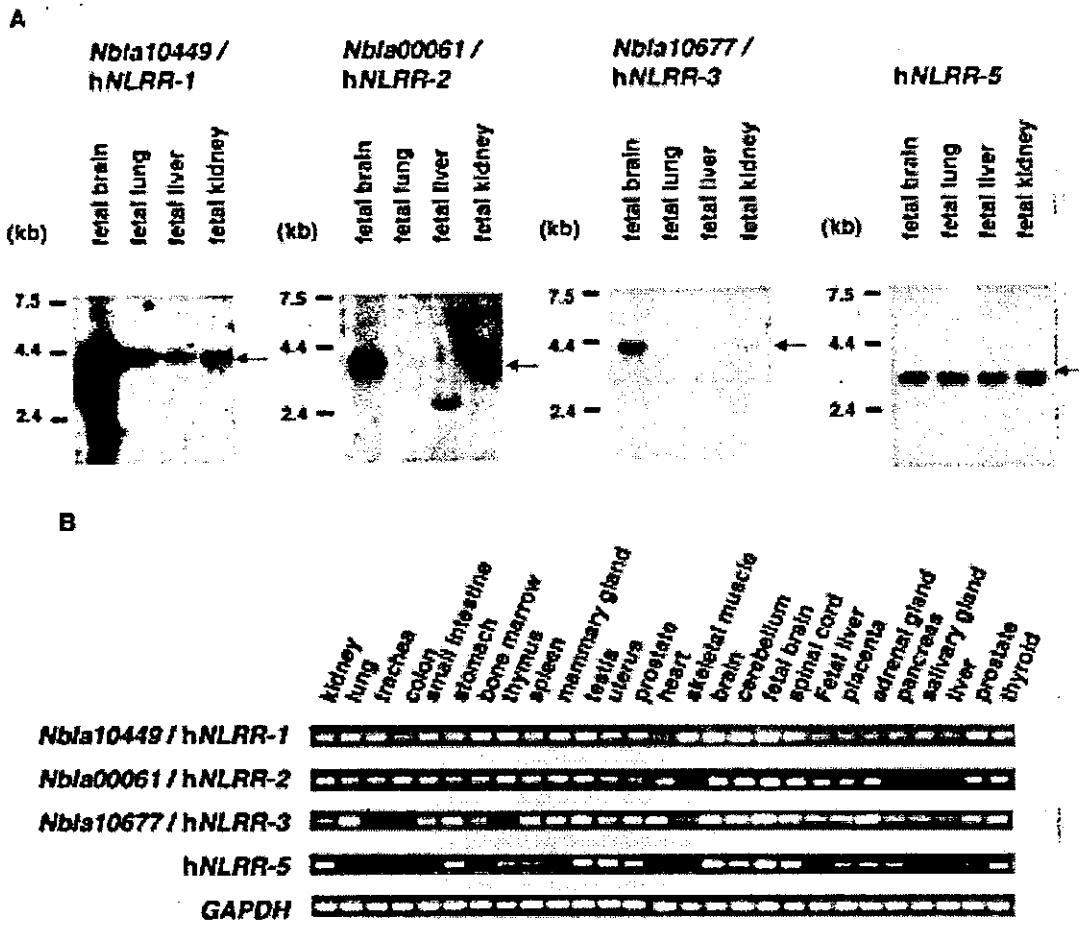

Figure 2. Expression of h*NLRR*s mRNA in human normal tissues. A, Northern blot analysis of h*NLRR*s mRNA in human fetal tissues. As a control for the amount of RNA, the same filter was rehybridized with ß-actin. B, Semi-quantitative RT-PCR of h*NLRR*s in multiple human tissues. Total RNA of 25 adult and 2 fetal tissues. As a control, same cDNA templates were amplified by *GAPDH* primers.

We then examined whether or not there was any genomic amplification of h*NLRR-1* or h*NLRR*-2 because that of *Nbla10449/hNLRR-1* was preferentially expressed in UF NBLs, and that of *GAC1/hNLRR-2* was reported to be amplified in the primary glioblastoma and anaplastic astrocytoma (15). However, our Southern blot analysis showed that neither of both genes was amplified in NBL cell lines so far examined (CHP134, IMR32, NB-9, NLF, TGW, NGP, NB69, NBL-S, SK-N-AS and SH-SY5Y) (data not shown). As regards the other cancer cell lines, expression of h*NLRR* family members was relatively restricted to the osteosarcoma and rhabdomyosarcoma cell lines (Fig. 3C). The low levels of h*NLRR*-3 and h*NLRR-5* expression were also seen in melanoma cell lines. Furthermore, expression of h*NLRR-2* was observed in the cell lines of colon, thyroid (medullary thyroid cancer), esophagus and lung. These results suggested that h*NLRR*s were preferentially expressed in the cell lines derived from neural crest cells.

Changes in expression of the NLRR family genes during NGF-induced differentiation and NGF-depletion-induced apoptosis in newborn mouse SCG neurons in primary culture. To investigate the role of NLRR family molecules in NGF/TrkA-mediated signaling, we next used newborn mouse SCG neurons, from which NBL is derived. As reported previously, NGF induced marked morphological differentiation of SCG neurons (14). NGF-induced neurite extension was observed on day 2 and was enhanced thereafter by increasing in number and length (Fig. 4A, NGF$^+$). The depletion of NGF by treating the cells with anti-NGF antibody induced neuronal programmed cell death (Fig. 4A, NGF$^-$). As shown in Fig. 4B, expression of m*NLRR-1* and m*NLRR-5* was down-regulated during NGF-induced neuronal differentiation, and was up-regulated after NGF deprivation (Fig. 4B). On the other hand, expression of m*NLRR-2* and m*NLRR-3* was slightly up-regulated when they were treated with NGF, and was significantly down-regulated after NGF deprivation (Fig. 4B), suggesting that expression of m*NLRR* genes might be related to the NGF signaling.

Prognostic significance of expression of Nbla10449/hNLRR-1 and Nbla10677/hNLRR-3 in primary neuroblastomas. To evaluate the clinical significance, expression of *Nbla10449/* h*NLRR-1* and *Nbla10677/*h*NLRR-3* in 99 NBLs was statistically analyzed. Table I gives the mean and standard error (SEM) of h*NLRR-1/Nbla10449* and h*NLRR-3/Nbla10677*

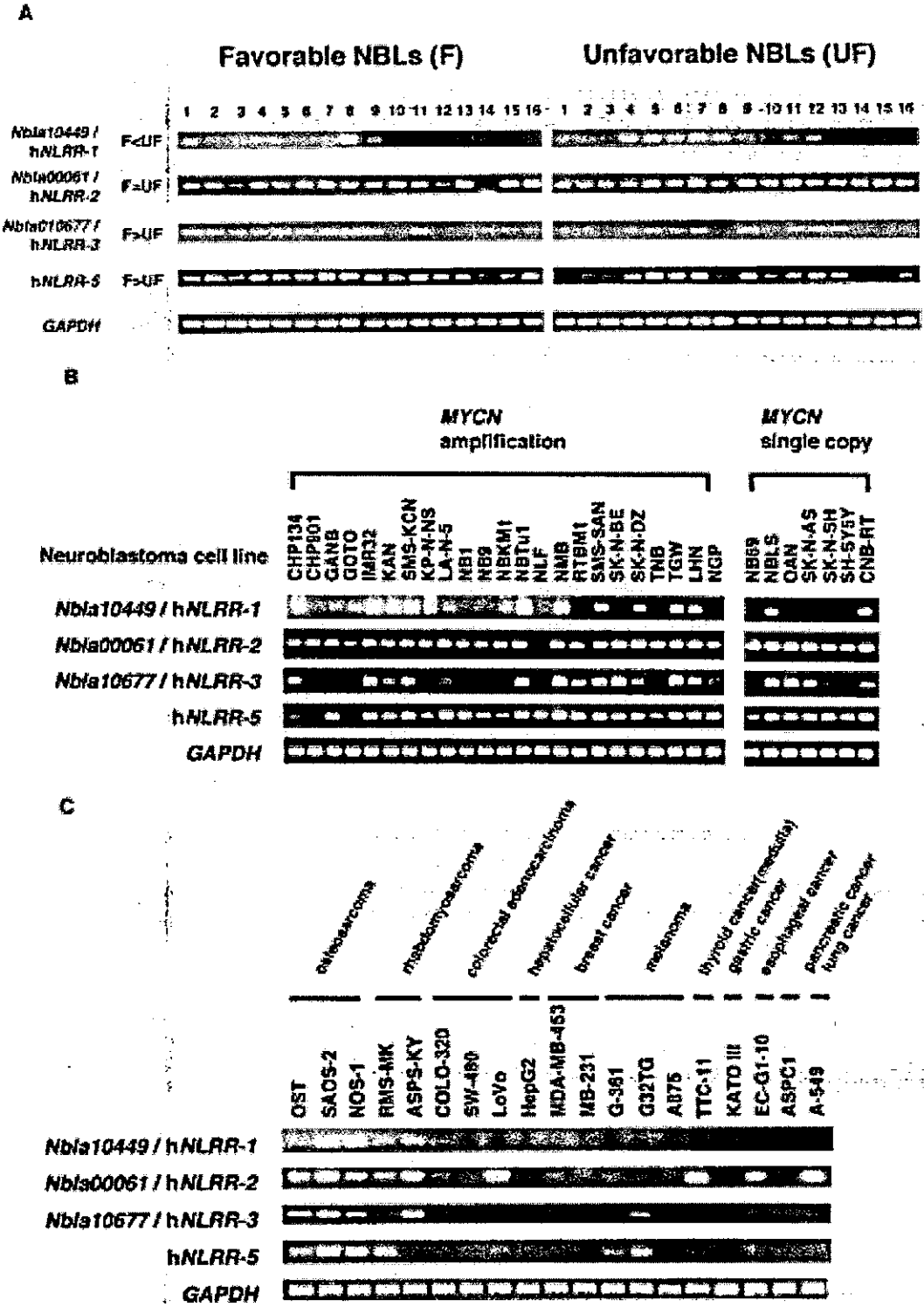

Figure 3. Expression of h*NLRR* family genes in primary NBLs, NBL cell lines and other cancer cell lines. A, Differential expression of h*NLRR* family genes in 16 favorable and 16 unfavorable NBLs. mRNA expression was detected by semi-quantitative RT-PCR procedure. The expression of *GAPDH* is shown as a control. Lanes 1-16: favorable NBLs (F, stage 1 or 2, with a single copy of *MYCN*), lanes 17-32: unfavorable NBLs (UF, stage 3 or 4, with *MYCN* amplification). B, Expression of h*NLRR*s mRNA in NBL cell lines. Twenty-three NBL cell lines with *MYCN* amplification and 7 cell lines with a single copy of *MYCN* were used for semi-quantitative RT-PCR as templates. C, Expression of h*NLRR*s mRNA in the other cancer cell lines. Semi-quantitative RT-PCR analysis was performed using cDNA and control *GAPDH* primers. Tumor origins are shown on the top.

expression by age, tumor stage, *TrkA* expression, *MYCN* copy number, origin, and mass screening. High expression of h*NLRR-1/Nbla10449* were significantly associated with >1 year of age (p=0.0001), advanced stage (p=0.0007), low expression of *TrkA* (p=0.011), *MYCN* amplification (p=0.0001) and sporadic tumors (p=0.0004), but not with the tumor origin (p=0.4). The results of log-rank test showed that a high level of h*NLRR-1/Nbla10449* expression was significantly associated

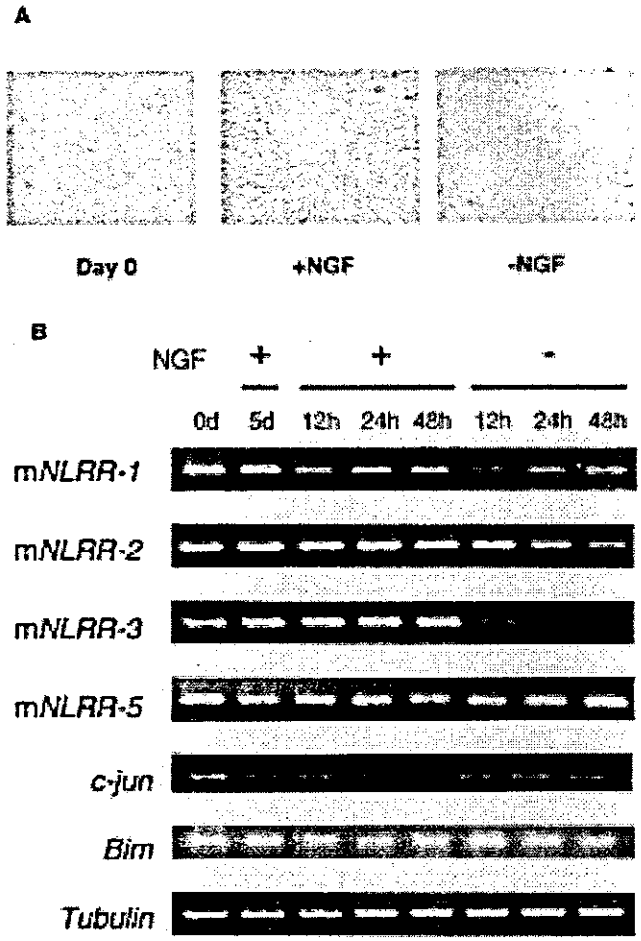

Figure 4. Changes in mRNA expression of mouse *NLRR* family genes in mouse superior cervical ganglion (SCG) cells treated with NGF in primary culture. A, Effect of NGF on newborn mouse SCG neurons in primary culture. The pictures were taken on day 0 and 5 (NGF^+) in the presence of 50 ng/ml NGF. NGF was then depleted from the medium by adding 1% v/v anti-NGF antibody for 36 h (NGF^-). B, Changes in expression of m*NLRR*s mRNA during NGF-induced differentiation and NGF depletion-induced apoptosis in newborn mouse SCG neurons in primary culture. SCG neurons were cultured for 5 days with NGF and then further cultured with or without NGF for 12, 24, 48 h. *c-jun* and *Bim*, positive control gene; Tubulin, used for standardization of the cDNA concentration.

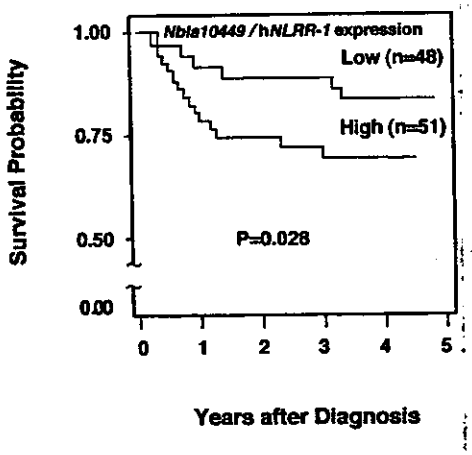

Figure 5. Kaplan-Meier survival curves for the 48 patients with low expression and the 51 patients with high expression.

with an unfavorable outcome (p=0.028). On the other hand, there was significant correlation between high levels of *Nbla10677/hNLRR-3* expression and younger age (p=0.0018), favorable stage (p=0.0007), high levels of *TrkA* expression (p=0.021), single copy of *MYCN* (p=0.0002) and the tumors found by mass screening (p=0.0049), but not with the tumor origin (p=0.33).

The univariate Cox regression was employed to examine the individual relationship of each variable to survival (Table II). These variables were: h*NLRR-1/Nbla10449* (log), h*NLRR-3/Nbla10677* (log), age (>1 year vs. <1 year), tumor stage (3+4 vs. 1+2+4s, *MYCN* copy number (1 copy vs. >1 copy), mass screening (+ vs. -), and origin (adrenal gland vs. others). Expression of h*NLRR-1/Nbla10449* (p=0.005), age (p<0.0005), *MYCN* copy number (p<0.0005), mass screening (p=0.001) were found to be statistically of prognostic importance. The results in Table II show that h*NLRR-1/Nbla10449* expression was an independent prognostic factor from age, *MYCN* copy number and mass screening in primary NBLs.

Discussion

In the present study, we identified the full-length human neuronal leucine-rich repeat protein (*NLRR*) family genes preferentially expressed in the nervous system and adrenal gland: *Nbla10449/hNLRR-1*, *Nbla00061/hNLRR-2/GAC1*, *Nbla10677/hNLRR-3* and h*NLRR-5*. In primary NBLs, the levels of h*NLRR-1* expression are significantly higher in the unfavorable subsets than those in the favorable tumors, whereas the expression pattern of h*NLRR-3* and h*NLRR-5* is the opposite. The results from the experiments using mouse SCG neurons treated with NGF in the primary culture have suggested that both m*NLRR-2* and *NLRR-3* are the molecules relating to promotion of neuronal survival or differentiation, while m*NLRR-1* and m*NLRR-5* function as those promoting cell growth or enhancing apoptosis. Furthermore, expression of h*NLRR-1* has been found as a significant indicator of poor outcome of NBLs, whereas that of h*NLRR-3* is associated with other favorable prognostic factors. Thus, hNLRR family members appear to differently regulate functions of neuronal cells as well as those of neuroblastoma.

A protein with leucine-rich repeat (LRR) domains was first identified in an α-2-glycoprotein of human serum (17). LRR-containing proteins represent a diverse group of molecules with different functions and cellular locations in a variety of organs. LRR domains provide an ideal conformation for binding to other proteins and this structure is thought to be involved in protein-protein interaction (10). Many LRR-containing proteins have been shown to function as cell-adhesion molecules or signaling receptors and are implicated in a variety of events in neural development. For example, adhesive LRR-containing proteins and small proteoglycans such as osteoinductive factor (OIF) bind various components of the extracellular matrix and growth factors. Interestingly, OIF binds the transforming growth factors, TGF-ß and TGF-ß2, and is involved in bone formation (18). The neurotrophin receptors, Trks, also possess the LRR domains in the extra-

Table I. Correlation between expression of *Nbla10449/hNLRR-1* or *Nbla10677/hNLRR-3* and other prognostic factors (Student's t-test).

Variable	No.	*Nbla10449/hNLRR-1* Mean ± SEM	*Nbla10449/hNLRR-1* p-value	*Nbla10677/hNLRR-3* Mean ± SEM	*Nbla10677/hNLRR-3* p-value
Age					
<1 year	63	0.84±0.21	0.0001	5.05±0.93	0.0018
>1 year	36	3.97±1.44		2.53±0.77	
Tumor stage					
1, 2, 4s	57	0.68±0.17	0.0007	5.36±1.00	0.0007
3, 4	42	3.74±1.25		2.48±0.68	
TrkA expression					
Low	45	3.50±1.17	0.011	3.13±0.77	0.021
High	54	0.71±0.18		4.97±1.02	
MYCN copy no.					
Amplified	29	5.19±1.75	0.0001	1.71±0.90	0.0002
Single	70	0.65±0.14		5.14±0.86	
Origin					
Adrenal gland	63	2.16±0.75	0.4	4.18±0.90	0.33
Others	36	1.67±0.79		4.06±0.93	
Mass screening					
+	54	0.67±0.18	0.0004	5.09±1.02	0.0049
-	45	3.55±1.17		2.98±0.76	

Table II. Cox regression models using *Nbla10449/hNLRR-1* expression and dichotomous factors of age, *TrkA* expression, *MYCN* amplification, and origin (n=99).

Model	Variable	p-value
A	*Nbla10449/hNLRR-1*	0.005
B	*Nbla10677/hNLRR-3*	0.15
C	Age (>1 vs. <1 year)	<0.005
D	*MYCN* (1 copy vs. amplification)	<0.005
E	Origin (adrenal gland vs. others)	0.079
F	Mass screening (+ vs. -)	0.001

cellular region. In *Drosophila*, some LRR domain-containing molecules such as toll, slit, connectin, chaoptin and tartan play an important role in regulating neural development (19-23).

The LRR motif includes highly hydrophobic amino acids and a repeat structure consisting of about 24 residues (20). NLRR family proteins contain in its extracellular region an immunoglobulin C-2 type domain and a fibronectin type III domain in addition to 11 sets of LRR motif (24). *NLRR* family genes were first isolated from a mouse brain cDNA library (16,25), and then 3 distinct isoforms (m*NLRR-1*, m*NLRR-2* and m*NLRR-3*) have been identified in zebrafish, *Xenopus*, mouse, rat and *Macaca facicularis* (16,24-26). The function of these NLRR proteins is poorly understood except that expression of m*NLRR-3* was increased after cortical brain injury (27) and that *rNLRR-3* expression is regulated through the Ras-MAPK signaling pathway in fibroblasts (28).

The deduced amino acid sequences of hNLRRs are highly conserved in the domains of LRR, LRRNT, LRRCT, Igc2 and FNIII, except that h*NLRR-5* does not have the FNIII domain. Many LRR proteins with LRRNT and LRRCT domains have been proposed to function in the regulation of neural differentiation and/or developmental processes as adhesive proteins and/or receptors (10). In addition to LRR, the Igc2 and FNIII domains in the extracellular region are often found in the molecules expressed in the central nervous system (26) and in several neuronal cell-adhesion molecules of the immunoglobulin superfamily such as N-CAM and L1 (29). Although hNLRRs and other NLRRs have no known signaling domain in the cytoplasmic region, a number of conserved stretches are found (Fig. 1). Especially, NLRR-1 and NLRR-3 have been shown to have a conserved stretch of 11 amino acids (ELYPPLINLWE) with 2 clathrin mediated endocytosis motifs, a tyrosine-based signal conforming to the YXRF motif (30,31), and a dileucine-type motif (32). Endocytosis and recycling mechanisms are relevant for cell adhesion molecules like integrins during cell migration (33,34).

Although the function of NLRR protein is poorly understood, there are some clues in recent reports. mNLRR-3 expression is increased in layers 2-3 in cerebral cortex after cortical injury, suggesting that this molecule plays a role in

the regulation of synaptic re-organization (27). zNLRR has also been proposed to have function as a neuronal-specific adhesion molecule or soluble ligand binding receptor during regeneration of the zebrafish central nervous system after injury, because retinal ganglion cells and descending spinal cord neurons strongly increased expression of *zNLRR* after axotomy in the adult (24).

The SCG/NGF system utilized in this study also provides a helpful hint to consider the neuronal function of hNLRRs. NLRR-1 may be involved in growth promotion in NBL by suppressing neuronal differentiation according to the result showing that the expression of m*NLRR-1* is down-regulated when the cells were treated with NGF. On the other hand, NLRR-3 may play a role in regulating differentiation to extend neurites and in neuronal survival of NBL cells since the expression of m*NLRR-3* was up-regulated by NGF and down-regulated after deprivation of NGF. These results are consistent with their differential expression pattern between favorable and unfavorable subsets of NBL.

In favorable NBLs as well as the cell lines with a single copy of *MYCN*, h*NLRR-1* expression was low as compared with the *MYCN*-amplified cells, suggesting that MYCN could influence the h*NLRR-1* expression. Interestingly, we have identified MYCN transcription factor-binding motifs (E-boxes) in the promoter region of the *NLRR-1* gene. Like h*NLRR-3*, h*NLRR-2* may also be involved in controlling neural cell survival as supposed from the result obtained in the NGF/SCG system. Ubiquitous h*NLRR-2* expression in NBLs suggests that h*NLRR-2* plays a role in maintaining cell survival. Of interest, h*NLRR-2* is often amplified in glioma as described below. h*NLRR-5* shows similar change in expression to h*NLRR-1* in the system of NGF-treated SCG neurons, albeit it is highly expressed in favorable NBLs. This suggests that hNLRR-5 may function as a proapoptotic molecule in NBL. Thus, each hNLRR member may have distinct biological function in NBL as well as neuronal cells. As the deduced intracellular region at the extreme C-terminus of hNLRR proteins has variable amino acid sequences, it may play a role in determining the differential function of hNLRR family receptors.

There are a few reports showing the relationship between LRR or NLRR and human cancer. *GAC1* (*hNLRR-2*), mapped to chromosome 1q32.1, is amplified and overexpressed in glioblastoma multiforme and anaplastic astrocytoma (15). Another report shows that expression of r*NLRR-3*, which was cloned by the subtractive screening using fibrosarcoma cells overexpressing c-Ha-ras, is regulated through the Ras-MAPK pathway, albeit the role in cancer cells is unknown (28). Trk family receptor tyrosine kinases have 3 LRRs in the extracellular domain, whose alteration can cause onco genic activation in some cancers (35). Interestingly, TrkA and TrkB also show an inverse expression pattern between favorable and unfavorable NBLs, that is very similar to the pattern of h*NLRR-1* and h*NLRR-3* expression. Since expression levels of TrkA and TrkB are powerful prognostic factors in NBLs, those of h*NLRR-1* and h*NLRR-3* may also be important in predicting the patient's outcome. Indeed, our present data suggest that expression of both hNLRR-1 and hNLRR-3 is inversely associated with the prognosis as well as other prognostic factors.

Acknowledgements

The authors thank Drs M. Fukumura, and H. Tsunobuchi for helpful discussions, Drs H. Kageyama and K. Miyazaki for experimental support, Dr S. Sakiyama for encouragement, and Ms. N. Sugimitsu and A. Morohashi for their excellent technical assistance. The authors also thank the following institutes for providing surgical samples: First Department of Surgery, Hokkaido University School of Medicine; Department of Pediatrics, National Sapporo Hospital; Department of Pediatric Surgery, Tohoku University School of Medicine; Department of Surgery, Gunma Children's Medical Center; Department of Pediatrics, Pediatric Surgery and General Surgery, Jichi Medical University; Department of Hematology and Oncology, Saitama Children's Medical Center; Department of Pediatrics, Juntendo University School of Medicine; Department of Surgery, Kiyose Metropolitan Children's Hospital; Department of Surgery and Pathology, Chiba Children's Hospital; Department of Pediatric Surgery, Chiba University School of Medicine; Department of Pediatric Surgery, Kimitsu Central Hospital; Department of Pediatric Surgery, Niigata University School of Medicine; Department of Pediatrics and Pediatric Surgery, Aichi Medical University; Department of Pediatrics, Kyoto Prefectural Medical University; Tumor Board, Hyogo Children's Hospital; Department of Pediatrics and Pediatric Surgery, Kagoshima University School of Medicine; Department of Pediatric Surgery, Showa University School of Medicine; Department of Pediatrics, Oita University School of Medicine; Department of Pediatric Surgery, Ohta General Hospital; Department of Pediatrics, Ichinomiya City Hospital; Department of Pediatric Surgery, Osaka City General Hospital; Department of Pediatrics, Nihon University School of Medicine Itabashi Hospital; Department of Pediatric Surgery, University of Tsukuba School of Medicine.

References

1. Bolande RP: The neurocristopathies. A unifying concept of disease arising in neural crest maldevelopement. Hum Pathol 5: 409-429, 1974.
2. Lo L, Morin X, Brunet JF and Anderson DJ: Specification of neurotransmitter identity by Phox2 proteins in neural crest stem cells. Neuron 22: 693-705, 1999.
3. Nakagawara A, Arima-Nakagawara M, Scavarda NJ, Azar CG, Cantor AB and Brodeur GM: Association between high levels of expression of the TRK gene and favorable outcome in human neuroblastoma. N Engl J Med 328: 847-854, 1993.
4. Nakagawara A, Azar CG, Scavarda NJ and Brodeur GM: Expression and function of TRK-B and BDNF in human neuroblastomas. Mol Cell Biol 14: 759-767, 1994.
5. Lasorella A, Noseda M, Beyna M, Yokota Y and Iavarone A: Id2 is a retinoblastoma protein target and mediates signaling by Myc oncoprotein. Nature 407: 592-598, 2000.
6. Ohira M, Shishikura T, Kawamoto T, Inuzuka H, Morohashi A, Takayasu H, Kageyama H, Takada N, Takahashi M, Sakiyama S, Suzuki Y, Sugano S, Kuma H, Nozawa I and Nakagawara A: Hunting the subset-specific genes of neuroblastoma: expression profiling and differential screening of the full-length-enriched oligo-capping cDNA libraries. Med Pediatr Oncol 35: 547-549, 2000.
7. Suzuki Y, Yoshitomo-Nakagawa K, Maruyama K, Suyama A and Sugano S: Construction and characterization of a full length-enriched and a 5'-end-enriched cDNA library. Gene 200: 149-156, 1997.

8. Ohira M, Morohashi A, Inuzuka H, Shishikura T, Kawamoto T, Kageyama T, Nakamura Y, Isogai E, Takayasu H, Sakiyama S, Suzuki Y, Sugano S, Goto T, Sato S and Nakagawara A: Expression profiling and characterization of 4200 genes cloned from primary neuroblastomas: identification of 305 genes differentially expressed between favorable and unfavorable subsets. Oncogene 22: 5525-5536, 2003.
9. Ohira M, Morohashi A, Nakamura Y, Isogai E, Furuya K, Hamano S, Machida T, Aoyama, Fukumura M, Miyazaki K, Suzuki Y, Sugano S, Hirato J and Nakagawara A: Neuroblastoma oligo-capping cDNA project: toward the understanding of the genesis and biology of neuroblastoma. Cancer Lett 197: 63-68, 2003.
10. Kobe B and Deisenhofer J: The leucine-rich repeat: a versatile binding motif. Trends Biochem Sci 19: 415-421, 1994.
11. Shimada H, Chatten J, Newton WA Jr, Sachs N, Hamoudi AB, Chiba T, Marsden HB and Misugi K: Histopathologic prognostic factors in neuroblastic tumors: definition of subtypes of ganglioneuroblastoma and an age-linked classification of neuroblastomas. J Natl Cancer Inst 73: 405-416, 1984.
12. Brodeur GM, Pritchard J, Berthold F, Carlsen NL, Castel V, Castelberry RP, De Bernardi B, Evans AE, Favrot M and Hedborg F: Revisions of the international criteria for neuroblastoma diagnosis, staging and response to treatment. J Clin Oncol 11: 1466-1477, 1993.
13. Kaneko M, Nishihira H, Mugishima H, Ohnuma N, Nakada K, Kawa K, Fukuzawa M, Suita S, Sera Y and Tsuchida Y: Stratification of treatment of stage 4 neuroblastoma patients based on N-myc amplification status. Study Group of Japan for Treatment of Advanced Neuroblastoma, Tokyo, Japan. Med Pediatr Oncol 31: 1-7, 1998.
14. Smith CJ, Johnson EM Jr, Osborne P, Freeman RS and Neveu I and Brachet P: NGF deprivation and neuronal degeneration trigger altered beta-amyloid precursor protein gene expression in the rat superior cervical ganglia *in vivo* and *in vitro*. Brain Res Mol Brain Res 17: 328-334, 1993.
15. Almeida A, Zhu XX, Vogt N, Tyagi R, Muleris M, Dutrillaux AM, Dutrillaux B, Ross D, Malfoy B and Hanash S: GAC1, a new member of the leucine-rich repeat superfamily on chromosome band 1q32.1, is amplified and overexpressed in malignant gliomas. Oncogene 16: 2997-3002, 1998.
16. Taguchi A, Wanaka A, Mori T, Matsumoto K, Imai Y, Tagaki T and Tohyama M: Molecular cloning of novel leucine-rich repeat proteins and their expression in the developing mouse nervous system. Brain Res Mol Brain Res 35: 31-40, 1996.
17. Takahashi N, Takahashi Y and Putnam FW: Periodicity of leucine and tandem repetition of a 24-amino acid segment in the primary structure of leucine-rich alpha 2-glycoprotein of human serum. Proc Natl Acad Sci USA 82: 1906-1910, 1985.
18. Kresse H, Hausser H and Schonherr E: Small proteoglycans. Experientia 49: 403-416, 1993.
19. Lemaitre B, Nicolas E, Michaut L, Reichhart JM and Hoffmann JA: The dorsoventral regulatory gene cassette spatzle/Toll/cactus controls the potent antifungal response in *Drosophila* adults. Cell 86: 973-983, 1996.
20. Rothberg JM, Jacobs JR, Goodman CS and Artavanis-Tsakonas S: Slit: an extracellular protein necessary for development of midline glia and commissural axon pathways contains both EGF and LRR domains. Genes Dev 4: 2169-2187, 1990.
21. Nose A, Mahajan VB and Goodman CS: Connectin: a homophilic cell adhesion molecule expressed on a subset of muscles and the motoneurons that innervate them in *Drosophila*. Cell 70: 553-567, 1992.
22. Krantz DE and Zipursky SL: *Drosophila chaoptin*, a member of the leucine-rich repeat family, is a photoreceptor cell-specific adhesion molecule. EMBO J 9: 1969-1977, 1990.
23. Chang Z, Price BD, Bockheim S, Boedigheimer MJ, Smith R and Laughon A: Molecular and genetic characterization of the *Drosophila tartan* gene. Dev Biol 160: 315-332, 1993.
24. Bormann P, Roth LW, Andel D, Ackermann M and Reinhard E: zfNLRR, a novel leucine-rich repeat protein is preferentially expressed during regeneration in zebrafish. Mol Cell Neurosci 13: 167-179, 1999.
25. Taniguchi H, Tohyama M and Takagi T: Cloning and expression of a novel gene for a protein with leucine-rich repeats in the developing mouse nervous system. Brain Res Mol Brain Res 36: 45-52, 1996.
26. Hayata T, Uochi T and Asashima M: Molecular cloning of XNLRR-1, a *Xenopus* homolog of mouse neuronal leucine-rich repeat protein expressed in the developing *Xenopus* nervous system. Gene 221: 159-166, 1998.
27. Ishii N, Wanaka A and Tohyama M: Increased expression of NLRR-3 mRNA after cortical brain injury in mouse. Brain Res Mol Brain Res 40: 148-152, 1996.
28. Fukamachi K, Matsuoka Y, Kitanaka C, Kuchino Y and Tsuda H: Rat neuronal leucine-rich repeat protein-3: cloning and regulation of the gene expression. Biochem Biophys Res Commun 287: 257-263, 2001.
29. Brummendorf T and Rathjen FG: Structure/function relationships of axon-associated adhesion receptors of the immunoglobulin superfamily. Curr Opin Neurobiol 6: 584-593, 1996.
30. Chen WJ, Goldstein JL and Brown MS: NPXY, a sequence often found in cytoplasmic tails, is required for coated pit-mediated internalization of the low density lipoprotein receptor. J Biol Chem 265: 3116-3123, 1990.
31. Collawn JF, Stangel M, Kuhn LA, Esekogwu V, Jing SQ, Trowbridge IS and Tainer JA: Transferrin receptor internalization sequence YXRF implicates a tight turn as the structural recognition motif for endocytosis. Cell 63: 1061-1072, 1990.
32. Kirchhausen T: Clathrin. Annu Rev Biochem 69: 699-727, 2000.
33. Lauffenburger DA and Horwitz AF: Cell migration: a physically integrated molecular process. Cell 84: 359-369, 1996.
34. Lawson MA and Maxfield FR: Ca(2+)- and calcineurin-dependent recycling of an integrin to the front of migrating neutrophils. Nature 377: 75-79, 1995.
35. Meakin SO and Shooter EM: The nerve growth factor family of receptors. Trends Neurosci 15: 323-231, 1992.

THE JOURNAL OF BIOLOGICAL CHEMISTRY
Vol. 279, No. 12, Issue of March 19, pp. 11327–11335, 2004
Printed in U.S.A.

NEDL1, a Novel Ubiquitin-protein Isopeptide Ligase for Dishevelled-1, Targets Mutant Superoxide Dismutase-1*

Received for publication, November 12, 2003, and in revised form, December 16, 2003
Published, JBC Papers in Press, December 18, 2003, DOI 10.1074/jbc.M312389200

Kou Miyazaki‡, Tomoyuki Fujita‡, Toshinori Ozaki‡, Chiaki Kato‡, Yuka Kurose‡, Maya Sakamoto‡, Shinsuke Kato§, Takeshi Goto¶, Yasuto Itoyama‖, Masashi Aoki‖, and Akira Nakagawara‡

From the ‡Division of Biochemistry, Chiba Cancer Center Research Institute, Chiba 260-8717, Japan, the §Division of Neuropathology, Institute of Neurological Sciences, Faculty of Medicine, Tottori University, Yonago 683-8504, Japan, ¶Hisamitsu Pharmaceutical Company Incorporated, Tokyo 100-622, Japan, and the ‖Department of Neurology, Tohoku University School of Medicine, Sendai 980-8574, Japan

Approximately 20% of familial amyotrophic lateral sclerosis (FALS) arises from germ-line mutations in the superoxide dismutase-1 (*SOD1*) gene. However, the molecular mechanisms underlying the process have been elusive. Here, we show that a neuronal homologous to E6AP carboxyl terminus (HECT)-type ubiquitin-protein isopeptide ligase (NEDL1) physically binds translocon-associated protein-δ and also binds and ubiquitinates mutant (but not wild-type) SOD1 proportionately to the disease severity caused by that particular mutant. Immunohistochemically, NEDL1 is present in the central region of the Lewy body-like hyaline inclusions in the spinal cord ventral horn motor neurons of both FALS patients and mutant *SOD1* transgenic mice. Two-hybrid screening for the physiological targets of NEDL1 has identified Dishevelled-1, one of the key transducers in the Wnt signaling pathway. Mutant SOD1 also interacted with Dishevelled-1 in the presence of NEDL1 and caused its dysfunction. Thus, our results suggest that an adverse interaction among misfolded SOD1, NEDL1, translocon-associated protein-δ, and Dishevelled-1 forms a ubiquitinated protein complex that is included in potentially cytotoxic protein aggregates and that mutually affects their functions, leading to motor neuron death in FALS.

Amyotrophic lateral sclerosis (ALS)[1] is a progressive, fatal, neurodegenerative disease that is characterized by selective loss of motor neurons in the spinal cord, brain stem, and motor cortex. The sporadic and familial forms of the disease have similar clinical and pathological features. About 10% of ALS cases are familial, and mutation of superoxide dismutase-1 (SOD1) is found in 20% of familial ALS (FALS) patients (1, 2). Mice that express mutant *SOD1* transgenes develop an age-dependent ALS phenotype independent of levels of dismutase activity, suggesting that FALS pathology is because of a toxic gain of function in SOD1 and that the abnormal protein structure of mutant SOD1 is critical in the pathogenesis of motor neuron death (3–6). Recently, proteasome expression and activity have been reported to decrease with age in the spinal cord (7, 8). Furthermore, mutant SOD1 turns over more rapidly than wild-type SOD1, and an inhibitor of proteasome action inhibits this turnover and thus selectively increases the steady-state level of mutant SOD1 (8). These results suggest the involvement of the ubiquitin-proteasome function in the cause of FALS. However, the biochemical nature of this gain-of-function mutation in SOD1 and the mechanism by which SOD1 mutations cause the degeneration of motor neurons have remained elusive.

We show here the identification of a novel HECT-type ubiquitin-protein isopeptide ligase (E3), NEDL1, which is expressed in neuronal tissues, including the spinal cord, and selectively binds to and ubiquitinates mutant (but not wild-type) SOD1. NEDL1 is physically associated with translocon-associated protein-δ (TRAP-δ), one of the endoplasmic reticulum (ER) translocon components that has previously been reported to bind mutant SOD1 (9, 10). Both NEDL1 and TRAP-δ form a complex with mutant SOD1, with the binding intensity among these proteins being roughly proportionate to the rapidity of progression of the associated FALS phenotype. Immunohistochemical study has shown that NEDL1 is positive in the Lewy body-like hyaline inclusions in the spinal cord motor neurons of both FALS patients and mutant *SOD1* transgenic mice. We have also found that NEDL1 targets Dishevelled-1 (Dvl1) for ubiquitination-mediated degradation and that mutant (but not wild-type) SOD1 affects the function of Dvl1. Our observations suggest that NEDL1 is a quality control E3 that recognizes mutant SOD1 to form a tight complex with the physiological targets of NEDL1 in motor neurons of FALS patients.

EXPERIMENTAL PROCEDURES

Cell Culture and Transfection—Human neuroblastoma-derived cells were grown in RPMI 1640 medium supplemented with 10% heat-inactivated fetal bovine serum, 100 units/ml penicillin, and 100 μg/ml streptomycin. COS-7 and Neuro2a cells were maintained in Dulbecco's modified Eagle's medium supplemented with 10% heat-inactivated fe-

* This work was supported in part by Hisamitsu Pharmaceutical Co. Inc. (to A. N.), by grants from the Ministry of Health, Labor, and Welfare of Japan (to A. N. and Y. I.), and by grants from the Ministry of Education, Culture, Sports, Science, and Technology of Japan (to A. N., Y. I., and M. A.). The costs of publication of this article were defrayed in part by the payment of page charges. This article must therefore be hereby marked "*advertisement*" in accordance with 18 U.S.C. Section 1734 solely to indicate this fact.

The nucleotide sequence(s) reported in this paper has been submitted to the GenBank™/EBI Data Bank with accession number(s) AB048365 (Nbla0078 and human NEDL1), AB002320 (KIAA0322), and AB083710 (mouse Nedl1).

** To whom correspondence should be addressed: Div. of Biochemistry, Chiba Cancer Center Research Inst., 666-2 Nitona, Chuoh-ku, Chiba 260-8717, Japan. Tel.: 81-43-264-5431; Fax: 81-43-265-4459; E-mail: akiranak@chiba-ccri.chuo.chiba.jp.

[1] The abbreviations used are: ALS, amyotrophic lateral sclerosis; FALS, familial amyotrophic lateral sclerosis; SOD1, superoxide dismutase-1; E3, ubiquitin-protein isopeptide ligase; NEDL1, NEDD4-like ubiquitin-protein ligase-1; TRAP-δ, translocon-associated protein-δ; ER, endoplasmic reticulum; Dvl1, Dishevelled-1; RT, reverse transcription; LBHI, Lewy body-like hyaline inclusion; JNK, c-Jun N-terminal kinase; HECT domain, homologous to E6AP carboxyl-terminus.

tal bovine serum, 100 units/ml penicillin, and 100 μg/ml streptomycin. All cells were maintained in a humidified 37 °C incubator with 5% CO_2. All transfections were carried out with LipofectAMINE Plus transfection reagent (Invitrogen) according to the manufacturer's instructions. In some experiments, transfected cells were treated with MG-132 for 30 min at a final concentration of 40 μM.

RNA Analysis—A human multiple tissue mRNA blot and a fetal human multiple mRNA blot (Invitrogen) were hybridized with a ^{32}P-labeled ApaI-ScaI restriction fragment of *NEDL1* cDNA under standard conditions. For reverse transcription (RT)-PCR analysis, cDNA derived from adult human neural system (BioChain Institute, Hayward, CA) was subjected to PCR amplification using the following primers: *NEDL1*, 5′-CCGATTTGAGATCACTTCCTCC-3′ (sense) and 5′-CCGCTTTCCATCAGGTTGTT-3′ (antisense); and glyceraldehyde-3-phosphate dehydrogenase, 5′-ACCTGACCTGCCGTCTAGAA-3′ (sense) and 5′-TCCACCACCCTGTTGCTGTA-3′ (antisense). The amplified products were separated by electrophoresis on a 1.5% agarose gel and visualized by ethidium bromide post-staining. Amplification of glyceraldehyde-3-phosphate dehydrogenase was used as an internal control.

In Vitro Ubiquitination Assays—*In vitro* ubiquitination assays were performed as follows. Reaction mixtures containing 0.5 μg of purified glutathione *S*-transferase fusion proteins, 0.25 μg of yeast ubiquitin-activating enzyme (*E1*) (BostonBiochem, Cambridge, MA), 1 μl of crude lysates from *Escherichia coli* expressing ubiquitin carrier proteins (*E2*), and 10 μg of bovine ubiquitin (Sigma) were incubated in 250 mM Tris-HCl (pH 7.6), 1.2 M NaCl, 50 mM ATP, 10 mM $MgCl_2$, and 30 mM dithiothreitol. Reactions were terminated after 2 h at 30 °C by the addition of SDS sample buffer. Samples were resolved by SDS-PAGE, transferred to membranes, and immunoblotted with anti-ubiquitin monoclonal antibody 1B3 (Medical & Biological Laboratories, Nagoya, Japan).

Immunofluorescence Staining—Cells grown on coverslips were processed for immunofluorescence. Briefly, cells were fixed in 3.7% formaldehyde, permeabilized in 0.2% Triton X-100, and finally incubated with anti-NEDL1 antibody (diluted 1:100). The primary antibody was detected with fluorescein isothiocyanate-conjugated goat anti-rabbit IgG (diluted 1:500; Jackson ImmunoResearch Laboratories, Inc., West Grove, PA). Images were taken using an Olympus confocal microscopy system.

Yeast Two-hybrid Screening—Yeast two-hybrid screening was performed using the Gal4-based Matchmaker two-hybrid system with the cDNA libraries derived from fetal human brain (first screening) and adult human brain (second screening) (Clontech, Palo Alto, CA). *Saccharomyces cerevisiae* CG1945 cells were transformed with pAS2–1-NEDL1-1 (amino acids 757–1114; first screening) or pAS2–1-NEDL1-2 (amino acids 382–1448; second screening), which did not activate the transcription of *lacZ* alone. The transformants were subsequently transformed with the cDNA library, and the *lacZ*-positive colonies were selected. The plasmid DNAs were extracted from these positive colonies, and their nucleotide sequences were determined.

Immunoprecipitation and Western Blot Analysis—Anti-NEDL1 and anti-TRAP-δ polyclonal antibodies were raised in rabbits against an NEDL1 oligopeptide (amino acids 460–482) and a TRAP-δ oligopeptide (amino acids 93–126), respectively. For immunoprecipitation, COS-7 or Neuro2a cells were cotransfected with the expression plasmids in various combinations and lysed 48 h later in 10 mM Tris-HCl (pH 7.8), 150 mM NaCl, 1% Nonidet P-40, 1 mM EDTA, and 1 mM phenylmethylsulfonyl fluoride supplemented with protease inhibitor mixture (Sigma). Whole cell lysates were immunoprecipitated with anti-NEDL1, anti-FLAG (M2; Sigma), or anti-Myc (9B11; Cell Signaling Technology, Beverly, MA) antibody. Immune complexes were recovered on protein G-Sepharose beads, eluted by boiling in Laemmli sample buffer, electrophoresed on SDS-polyacrylamide gel, and then transferred to a polyvinylidene difluoride membrane (Immobilon, Millipore Corp., Bedford, MA) by electroblotting. For ubiquitination experiments, cell lysis was performed in radioimmune precipitation assay buffer (10 mM Tris-HCl (pH 7.4), 150 mM NaCl, 1% Nonidet P-40, 0.1% sodium deoxycholate, 0.1% SDS, and 1 mM EDTA), followed by strong sonication and freeze-thaw. The membrane was probed with the indicated primary antibodies and then incubated with the appropriate secondary antibodies labeled with horseradish peroxidase (Jackson ImmunoResearch Laboratories, Inc. and Southern Biotechnology Associates, Inc., Birmingham, AL). Immunoreactive bands were detected by the enhanced chemiluminescence technique (ECL, Amersham Biosciences). For the detection of c-Jun phosphorylation, we used anti-c-Jun (sc-45, Santa Cruz Biotechnology, Santa Cruz, CA) or anti-phospho-Ser^{63} c-Jun (Cell Signaling Technology) antibody.

Cloning of Human NEDL1 cDNA—A forward primer (5′-GGTTTTTAGGCCTGGCCGCC-3′) and a reverse primer (5′-CAATGAGGTACATGCCAATCC-3′) were used to amplify the 5′-part of the *NEDL1* cDNA using cDNA libraries derived from human neuroblastoma and fetal human brain (Stratagene, La Jolla, CA) as templates. The full-length human *NEDL1* cDNA was generated by fusion of the PCR-amplified fragment (nucleotides +1 to +68, where position +1 represents the translation initiation site) and the *KIAA0322* cDNA (a gift from T. Nagase, Kazusa DNA Institute). Gel electrophoresis and Western blot analysis were carried out as described above.

Expression Constructs—The mammalian expression plasmids for hemagglutinin-tagged and His_6-tagged ubiquitin were kind gifts of D. Bohmann. The full-length *NEDL1* cDNA was inserted into the mammalian expression plasmid pEF1/His (Invitrogen) or pIRESpuro2 (Clontech). cDNAs encoding wild-type and mutant forms of SOD1 were fused to the FLAG or Myc epitope tag sequence at their C termini and subcloned into pIRESpuro2. Similarly, the FLAG or Myc epitope tag sequence was attached to the C terminus of TRAP-δ. Also similarly, the FLAG or Myc epitope tag sequence was attached to the N terminus of Dvl1. Coding sequences were verified by automated DNA sequencing.

Protein Stability Experiments—Neuro2a cells were transfected with the expression plasmid for the wild-type or mutant form of SOD1 with or without the NEDL1 expression plasmid. Twenty-four hours after transfection, cycloheximide (50 μg/ml) was added to the culture medium, and the cells were harvested at the indicated time points by lysis in radioimmune precipitation assay buffer. The protein concentrations were determined using the Bradford protein assay system (Bio-Rad) according to the instructions of the manufacturer.

Immunohistochemistry—The immunohistochemical studies were performed as described previously using affinity-purified rabbit anti-NEDL1 antibody (11). Patient tissues were obtained at autopsy from two FALS siblings from a Japanese family. The clinical course of the sister, who died at age 46, was 18 months (case 1), and that of the brother, who died at age 65, was 11 years (case 2) (11). The *SOD1* gene was mutated with a 2-bp deletion at codon 126 (11, 12). Normal spinal cord tissues were obtained from three neurologically and neuropathologically normal individuals. The same study was performed on spinal cord tissues from three normal rats and a transgenic ALS rat carrying a mutant allele of the human *SOD1* gene (H46R) (13). These mice were killed at 180 days. As a negative control, some sections were incubated with anti-NEDL1 antibody that had been pre-absorbed with an excess of NEDL1 antigen. Bound antibodies were visualized by the avidin-biotin-immunoperoxidase complex method.

RESULTS

Cloning and Expression of the NEDL1 E3 Gene—To detect novel molecules that are important in regulating neuronal programmed cell death, we constructed oligo-capping cDNA libraries from a mixture of three fresh human neuroblastoma tissues (stages 1 and 2) that were undergoing gradual spontaneous regression, probably by neuronal apoptosis (14). Screening of 1152 novel genes by RT-PCR revealed that 194 genes were expressed differentially in regressing neuroblastomas with favorable prognosis and in aggressive tumors with poor prognosis. Among these genes, we found a partial cDNA sequence with an HECT-like domain (*Nbla0078*) that partially matched the *KIAA0322* gene. Because *KIAA0322* lacks a 5′-coding region, we used a genome-based PCR procedure to clone the corresponding full-length cDNA. This is predicted to encode a protein product of 1585 amino acids with homology to NEDD4 E3 (15, 16), which includes a C2 domain at the N-terminal region supposed to mediate its membrane localization in a calcium-dependent manner, two WW motifs important for protein-protein interaction through binding to specific proline-rich clusters, and a conserved catalytic HECT domain at the C terminus (Fig. 1*A*). We named this novel ligase, which mapped to chromosome 7p13, NEDL1 (NEDD4-like ubiquitin-protein ligase-1). We also cloned the mouse counterpart of *NEDL1* cDNA, whose amino acid sequence is 78% identical to the human sequence. Tissue-specific expression of *NEDL1* mRNA of ~10 and 7 kb in size was observed, with predominant expression in adult and fetal brains as examined by Northern blot analysis (Fig. 1*B*). Its

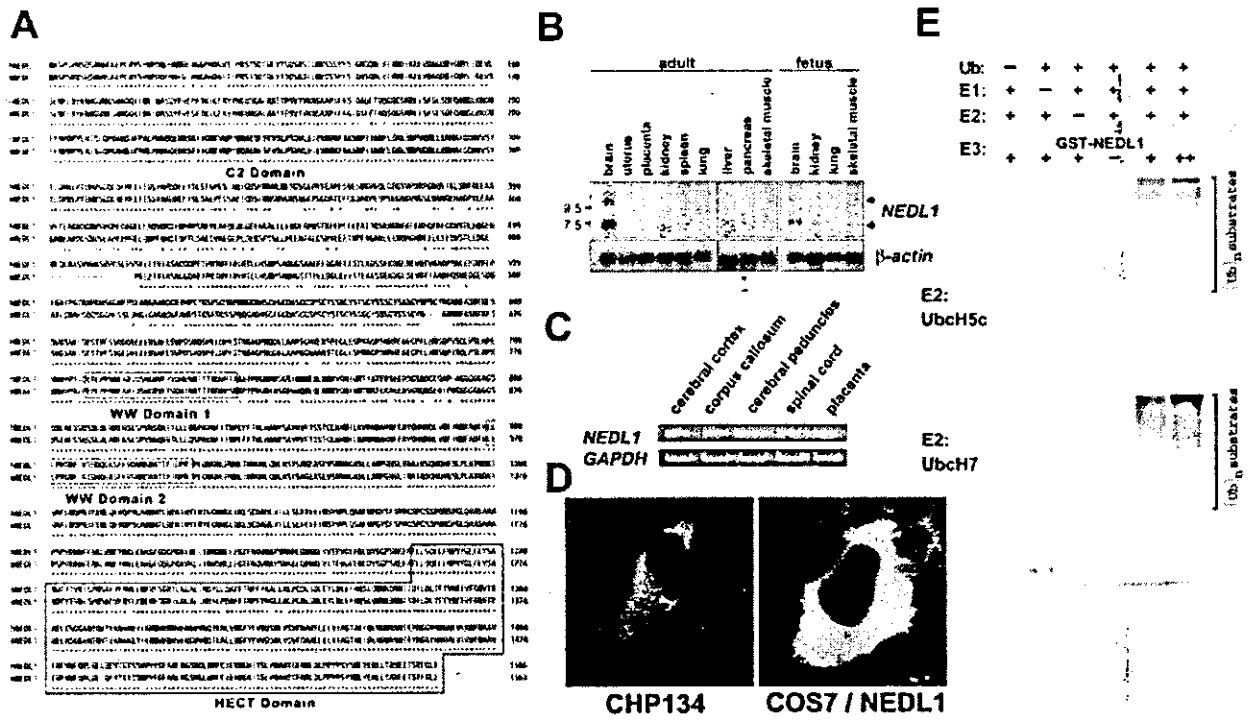

FIG. 1. **Amino acid sequence, brain-specific expression, and subcellular localization of NEDL1 E3.** *A*, alignment of conserved amino acid sequences of human NEDL1 (*hNEDL1*) and its mouse homolog (*mNEDL1*). *Numbers* on the right indicate the number of residues to the initiator methionine. The C2 domain (*shaded*), two WW domains (*dashed boxes*), and the HECT domain (*solid box*) are indicated. *B*, brain-specific expression of *NEDL1* mRNA. Total RNAs derived from the indicated adult (*left panel*) and fetal (*right panel*) human tissues were analyzed by Northern blotting using a ^{32}P-labeled human *NEDL1* cDNA restriction fragment as a probe. Control hybridization with a human β-actin cDNA probe verified the equal amount of RNA loaded. *C*, expression of *NEDL1* in human brain subsections. Total RNA from the cerebral cortex, corpus callosum, cerebral peduncles, spinal cord, or placenta was subjected to RT-PCR using specific primers for *NEDL1* or glyceraldehyde-3-phosphate dehydrogenase (*GAPDH*). RT-PCR analysis for *NEDL1* in the placenta provided a negative control. Amplification of glyceraldehyde-3-phosphate dehydrogenase was used as an internal control. *D*, confocal microscopic images of human neuroblastoma CHP134 cells (*left panel*) and COS-7 cells transfected with an expression plasmid for NEDL1 (*right panel*). Cells were subjected to immunofluorescence analysis using rabbit anti-NEDL1 polyclonal antibody, followed by fluorescein isothiocyanate-conjugated anti-mouse IgG. E, *in vitro* ubiquitination assays showing that NEDL1 has a ubiquitin-protein ligase activity. The degree of ubiquitination was increased in an NEDL1-dependent manner. In this assay, yeast ubiquitin-activating enzyme (*E1*), bacterially expressed ubiquitin carrier protein (*E2*; UbcH5C or UbcH7), and bacterial lysates were incubated in the presence or absence of increasing amounts of glutathione *S*-transferase (*GST*)-NEDL1. Polyubiquitinated bacterial proteins appeared to migrate in a high molecular mass complex. *Ub*, ubiquitin.

expression was also weakly detected in adult kidney, where the size of the expressed transcript appeared to be <7 kb. Expression of *NEDL1* in specific regions of the nervous system was further confirmed in the cerebral cortex, corpus callosum, cerebral peduncles, and spinal cord by RT-PCR (Fig. 1*C*). Thus, NEDL1 is a novel HECT-type E3 preferentially expressed in neuronal tissues, including the spinal cord. Using a specific anti-NEDL1 polyclonal antibody that we generated, we localized NEDL1 primarily to the cytoplasm in both intact human neuroblastoma CHP134 cells and COS-7 cells transiently expressing NEDL1 (Fig. 1*D*). The *in vitro* system containing UbcH5c or UbcH7 demonstrated that NEDL1 has a ubiquitin-protein ligase activity (Fig. 1*E*).

NEDL1 Physically Interacts with TRAP-δ and Mutant SOD1—We then sought protein-binding partners of NEDL1 by yeast two-hybrid screening using the region including two WW protein interaction domains (amino acids 757–1114) as bait. Of 96 positive clones subjected to DNA sequencing, one was a full-length cDNA for TRAP-δ; this was of considerable interest, as TRAP-δ was previously reported to bind mutant (G85R and G93A), but not wild-type, SOD1 (9). TRAP-δ is a protein component of the translocon in the ER membrane (10). We therefore examined the interaction among NEDL1, TRAP-δ, and SOD1 by an immunoprecipitation assay after cotransfecting the corresponding expression constructs into COS-7 cells. As shown in Fig. 2 (*A* and *B*), NEDL1 was physically associated with both exogenous and endogenous TRAP-δ probably through the region of two WW domains, as originally suggested by the result of two-hybrid screening. Surprisingly, NEDL1 bound to mutant (but not wild-type) SOD1 (Fig. 2*C*). Furthermore, the degree of binding between NEDL1 and different mutant SOD1 proteins was roughly proportionate to the rapidity of progression (time from clinical onset to death) of the associated FALS phenotype (17–23). For example, two mutant SOD1 proteins associated with an extremely rapid clinical course (C6F and A4V) interacted very strongly with NEDL1. By contrast, the binding of NEDL1 to other mutants was less striking and decreased proportionately to the falloff of disease severity corresponding to those mutants. Of further interest, like the NEDL1-mutant SOD1 interaction, the binding intensity between TRAP-δ and mutant SOD1 was also dependent on the disease severity (Fig. 2*D*). These observations suggest that NEDL1 and TRAP-δ are normally associated with each other, but that misfolded mutant SOD1 makes a complex with them. Such a complex is not formed with wild-type SOD1. The experiments using the *in vitro* translated proteins suggested that association of mutant SOD1 and TRAP-δ was direct (data not shown). It therefore appears that mutant SOD1 forms tightly bound protein complexes with NEDL1 and TRAP-δ and that the tightness of binding in the complex is determined in part by

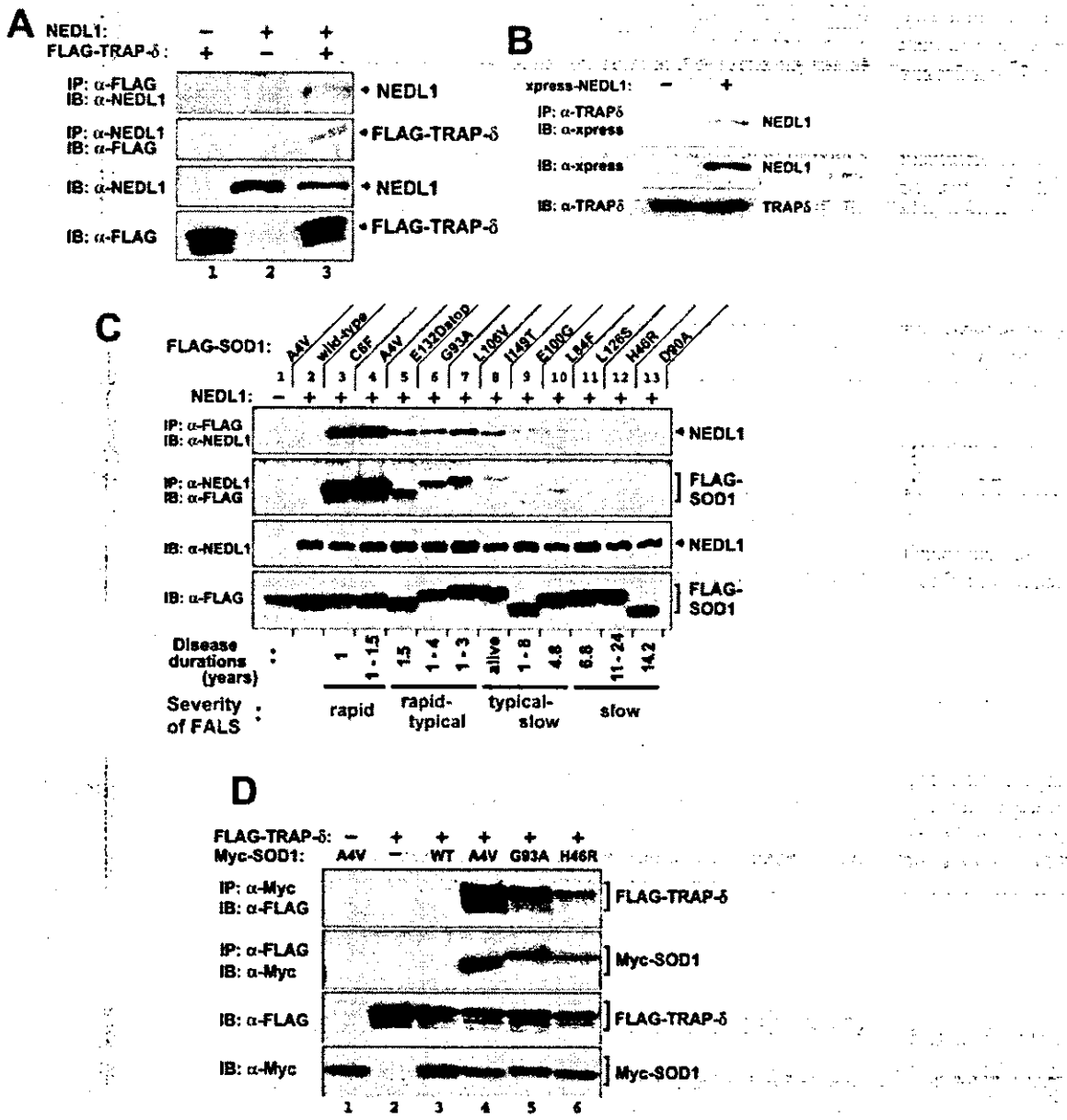

FIG. 2. **NEDL1 interacts with TRAP-δ and FALS-associated mutant forms of SOD1, but not with wild-type SOD1.** *A*, NEDL1 interacts with TRAP-δ. COS-7 cells were cotransfected with the indicated expression plasmids, and whole cell lysates were immunoprecipitated (*IP*) with anti-FLAG (*first panel*) or anti-NEDL1 (*second panel*) antibody. Immunoprecipitates were analyzed by immunoblotting (*IB*) using the indicated antibodies. Whole cell lysates were analyzed for expression levels of each protein by immunoblot analysis (*third* and *fourth panels*). Detection was performed with horseradish peroxidase-conjugated secondary antibodies. *B*, NEDL1 also binds to endogenous TRAP-δ. *C*, interaction between NEDL1 and mutant SOD1. Whole cell lysates from COS-7 cells overexpressing NEDL1 and one of the FLAG-tagged SOD1 mutants or wild-type SOD1 were immunoprecipitated with anti-FLAG (*first panel*) or anti-NEDL1 (*second panel*) antibody and then immunoblotted with anti-NEDL1 or anti-FLAG antibody, respectively. The expression of NEDL1 or FLAG-tagged SOD1 mutants was analyzed by immunoblotting using anti-NEDL1 (*third panel*) or anti-FLAG (*fourth panel*) antibody, respectively. Patients carrying the SOD1(C6F) and SOD1(A4V) mutations have a rapid clinical course, whereas mutant SOD1(L126S), SOD1(H46R), or SOD1(D90A) is associated with a slow clinical course. *D*, interaction of TRAP-δ with mutant SOD1. COS-7 cells were transiently cotransfected with the expression plasmid for FLAG-tagged TRAP-δ and the expression plasmid encoding one of the Myc-tagged SOD1 mutants or wild-type (*WT*) SOD1. Whole cell lysates were immunoprecipitated with anti-Myc (*first panel*) or anti-FLAG (*second panel*) antibody, followed by immunoblotting with anti-FLAG or anti-Myc antibody, respectively. The levels of overexpression of FLAG-tagged TRAP-δ (*third panel*) and Myc-tagged SOD1 (*fourth panel*) were analyzed by immunoblotting using anti-FLAG and anti-Myc antibodies, respectively.

properties of the mutant enzyme that also modulate disease severity of the resulting ALS phenotype. Such complexes do not form in cells with wild-type SOD1.

Determination of the Interaction Domains—We next examined the domains of NEDL1 required for formation of the SOD1·NEDL1·TRAP-δ complex. We generated various constructs of NEDL1 with deletions of each domain. Fig. 3 shows the results of immunoprecipitation assay for the association between deletion mutants of NEDL1 and mutant SOD1(G93A). Mutant SOD1 bound weakly to NEDL1 lacking WW domain-1 (Fig. 3*A*), suggesting that WW domain-1 and its surrounding portion are the region involved in their interaction. Immuno-

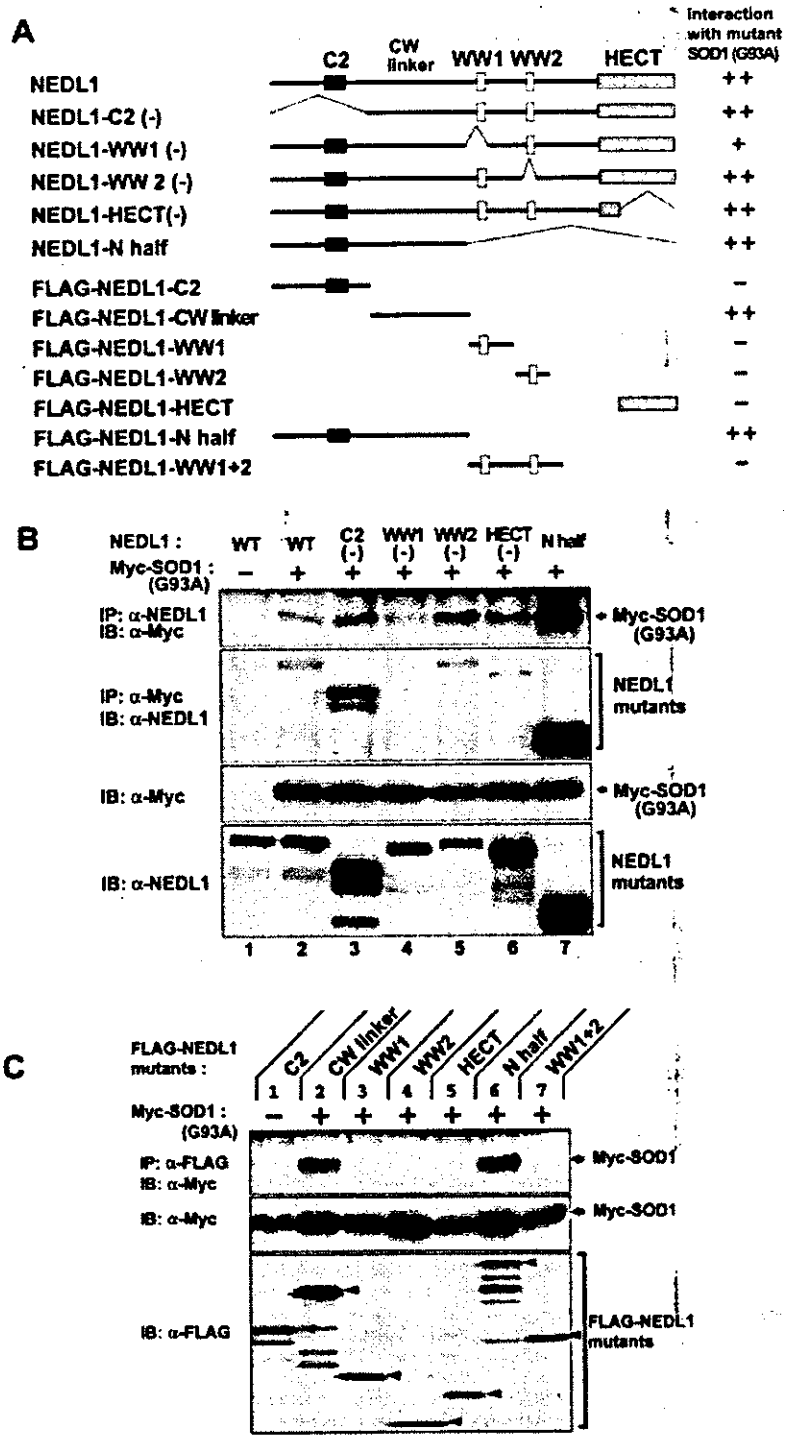

FIG. 3. **The region of NEDL1 between the C2 domain and WW domain-1 is required for interaction with mutant SOD1.** *A*, schematic illustration of wild-type NEDL1 and a series of deletion mutants of NEDL1. *CW linker* indicates the region between the C2 domain and WW domain-1 (*WW1*). *B* and *C*, immunoprecipitation and immunoblot analyses. In *B*, Myc-tagged mutant SOD1(G93A) was overexpressed together with wild-type (*WT*) NEDL1 or the indicated deletion mutants of NEDL1 in COS-7 cells. Whole cell lysates were immunoprecipitated (*IP*) with anti-NEDL1 (*first panel*) or anti-Myc (*second panel*) antibody, followed by immunoblotting (*IB*) with anti-Myc or anti-NEDL1 antibody, respectively. The expression levels of each protein were analyzed by immunoblotting using the indicated antibodies (*third* and *fourth panels*). In *C*, whole cell lysates were immunoprecipitated with anti-FLAG antibody and then immunoblotted with anti-Myc antibody (*upper panel*). Whole lysates were also analyzed by Western blotting for each protein (*middle* and *lower panels*).

precipitation analysis using the specific regions of NEDL1 clearly showed that the region between the C2 domain and WW domain-1 (CW linker region) is necessary for binding to mutant SOD1(G93A). Mutant SOD1(A4V) was also associated with NEDL1 through the same region, and TRAP-δ bound to the two WW domains of NEDL1 (data not shown).

NEDL1 Ubiquitinates Mutant SOD1 for Degradation Depending on the Disease Severity of FALS—Because NEDL1 is an E3, we next tested whether it ubiquitinates TRAP-δ and mutant SOD1 for degradation. As shown in Fig. 4*A*, NEDL1 clearly ubiquitinated mutant SOD1(A4V), but not TRAP-δ (data not shown). Furthermore, the degree of ubiquitination of mutant SOD1 by NEDL1 was dependent on the disease severity of FALS (A4V > G93A > H46R) (Fig. 4*A*). Fig. 4*B* shows the time course of degradation of wild-type and mutant SOD1 in the presence or absence of NEDL1. As reported previously (46), mutant SOD1 was degraded more rapidly than wild-type SOD1. NEDL1 did not affect wild-type SOD1 degradation. As expected from the co-immunoprecipitation and ubiquitination analyses, degradation of mutant SOD1 was stimulated by NEDL1 proportionately to the disease severity of FALS caused by the particular SOD1 mutant (A4V > G93A > H46R ≥

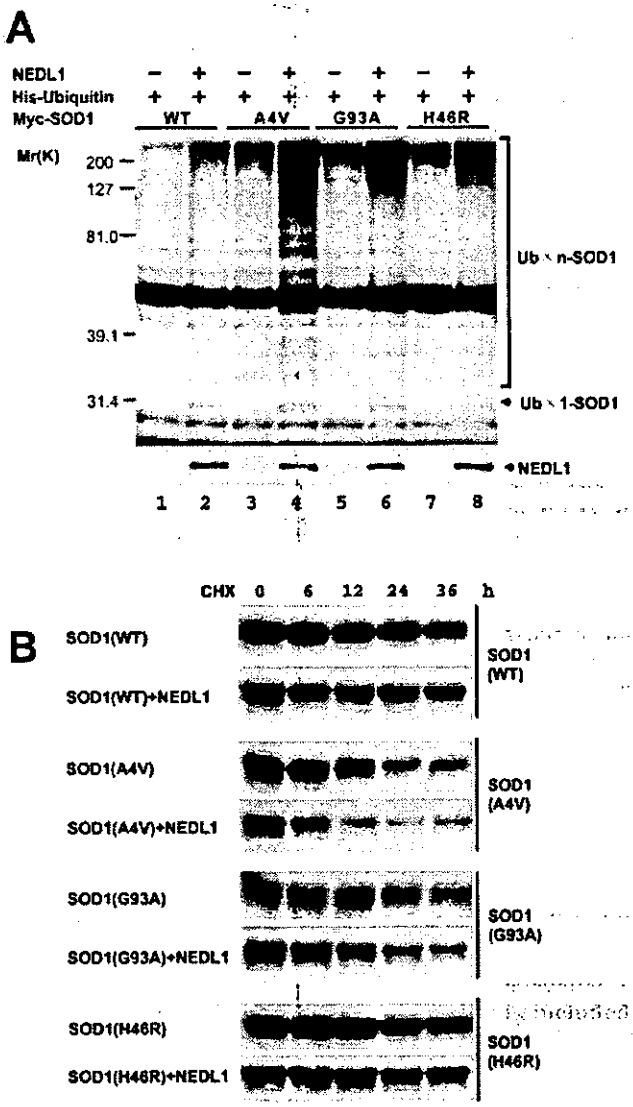

FIG. 4. **NEDL1-dependent ubiquitination and degradation of mutant forms of SOD1 correlate broadly with their respective clinical phenotypes.** *A*, NEDL1 ubiquitinates mutant SOD1 in a mutant type-dependent manner. COS-7 cells were transiently cotransfected with the indicated expression plasmids. Whole cell lysates from transfected COS-7 cells were immunoprecipitated with anti-Myc antibody, and immunoprecipitates were analyzed by Western blotting with anti-ubiquitin (*Ub*) antibody (*upper panel*). The *bracket* indicates slowly migrating ubiquitinated forms of SOD1. Whole cell lysates were analyzed by immunoblotting with anti-NEDL1 antibody to confirm the expression of transfected NEDL1 (*lower panel*). The running positions of molecular weight markers are indicated on the left. *B*, half-lives of wild-type (*WT*) and mutant SOD1 proteins in the presence or absence of NEDL1. Cell lysates were harvested from Neuro2a cells transfected with *SOD1* alone or with *SOD1* plus *NEDL1* at different time points as indicated after the addition of cycloheximide (*CHX*; final concentration of 50 μg/ml) and were analyzed for SOD1 protein levels by Western blotting with anti-FLAG antibody. In the presence of NEDL1, the half-lives of various mutant SOD1 proteins were reduced also roughly dependent on the disease severity of FALS (A4V > G93A > H46R).

wild-type). Thus, NEDL1 targeted mutant SOD1 for ubiquitin-mediated degradation in the cell in parallel with the binding intensity.

Immunohistochemistry—One of the characteristic cytopathological changes of mutant SOD1-linked FALS is the formation of neuronal Lewy body-like hyaline inclusions (LBHIs) that contain aggregates of SOD1 and ubiquitin (24). We therefore

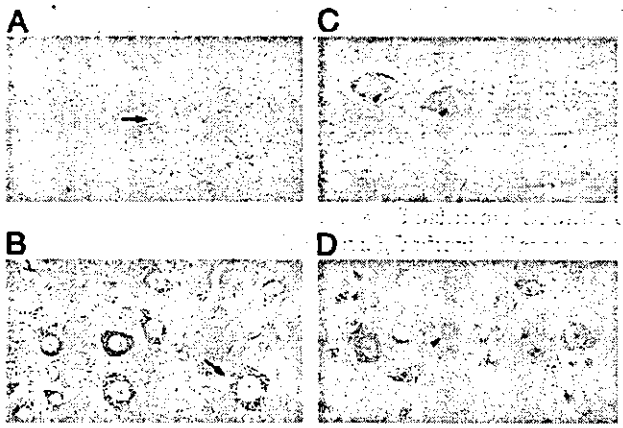

FIG. 5. **NEDL1 immunohistochemical analyses.** *A*, immunohistochemical analysis of NEDL1 in normal human spinal cord. NEDL1-positive anterior horn cells are evident (*arrow*), although the immunoreactivity for NEDL1 is somewhat faint. There was no counterstaining. Magnification ×520. *B*, NEDL1 immunohistochemistry in normal mouse spinal cord. Normal anterior horn cells are positive for NEDL1 (*arrow*). The section was counterstained with hematoxylin. Magnification ×750. *C*, immunostaining for NEDL1 in spinal cord LBHIs from an FALS patient with a frameshift 126 mutation in the *SOD1* gene. The NEDL1-positive reaction products were mostly restricted to the cores of the core and halo-type LBHIs (*arrowheads*). In the LBHI-bearing neurons and residual neurons, the antibody to NEDL1 also stained the neuronal cell body. There was no counterstaining. Magnification ×540. *D*, NEDL1 immunostaining in a spinal cord LBHI from an *SOD1*(H46R) transgenic mouse. An ill defined LBHI in the *SOD1*(H46R) transgenic mouse was positive for NEDL1; this ill defined LBHI shows a diffuse staining pattern (*arrowhead*). The staining intensity in the residual neurons stained by anti-NEDL1 antibody varied from neuron to neuron. The section was counterstained with hematoxylin. Magnification ×770.

performed immunostaining to determine whether the NEDL1 protein is included within the LBHIs of the spinal cord motor neurons obtained from two siblings with FALS caused by frameshift 126 mutation of SOD1 (11, 12). One case had neuropathological findings compatible with FALS with posterior column involvement, whereas the other had multisystem degeneration in addition to motor neuron disturbance. We also performed NEDL1 immunostaining in specimens obtained from mutant *SOD1*(H46R) transgenic mice at 180 days, by which time they show clinical motor signs in the hind limbs (13). The specificity of the NEDL1 staining was confirmed by pretreating the specimens with an excess of NEDL1 antigen. NEDL1 immunoreactivity in the spinal cords of the human control cases was identical to that of normal mice: immunoreactivity was identified predominantly in the cytoplasm of the neurons of the spinal cords (Fig. 5, *A* and *B*). The LBHIs in the anterior horn cells of two FALS patients and transgenic mice showed equivalent immunoreactivity for NEDL1. Although the intensity of NEDL1 immunoreactivity in neuronal LBHIs varied, most of the LBHIs were immunoreactive for NEDL1 (Fig. 5, *C* and *D*). The reaction products were generally restricted to the cores of the core and halo-type LBHIs that showed eosinophilic cores with pale peripheral halos upon hematoxylin and eosin staining (Fig. 5*C*); by contrast, immunopositive NEDL1 in ill defined LBHIs was distributed throughout the inclusions (Fig. 5*D*). NEDL1 immunoreactivity in the residual neurons in humans and mice was identified primarily in cell bodies. Thus, NEDL1 immunostaining was clearly positive in the FALS-related LBHIs that were also positive for ubiquitin and SOD1 (data not shown).

NEDL1 Targets Dishevelled-1 for Ubiquitin-mediated Protein Degradation—We next hypothesized that the physiological function of NEDL1 to mediate ubiquitination is interfered with

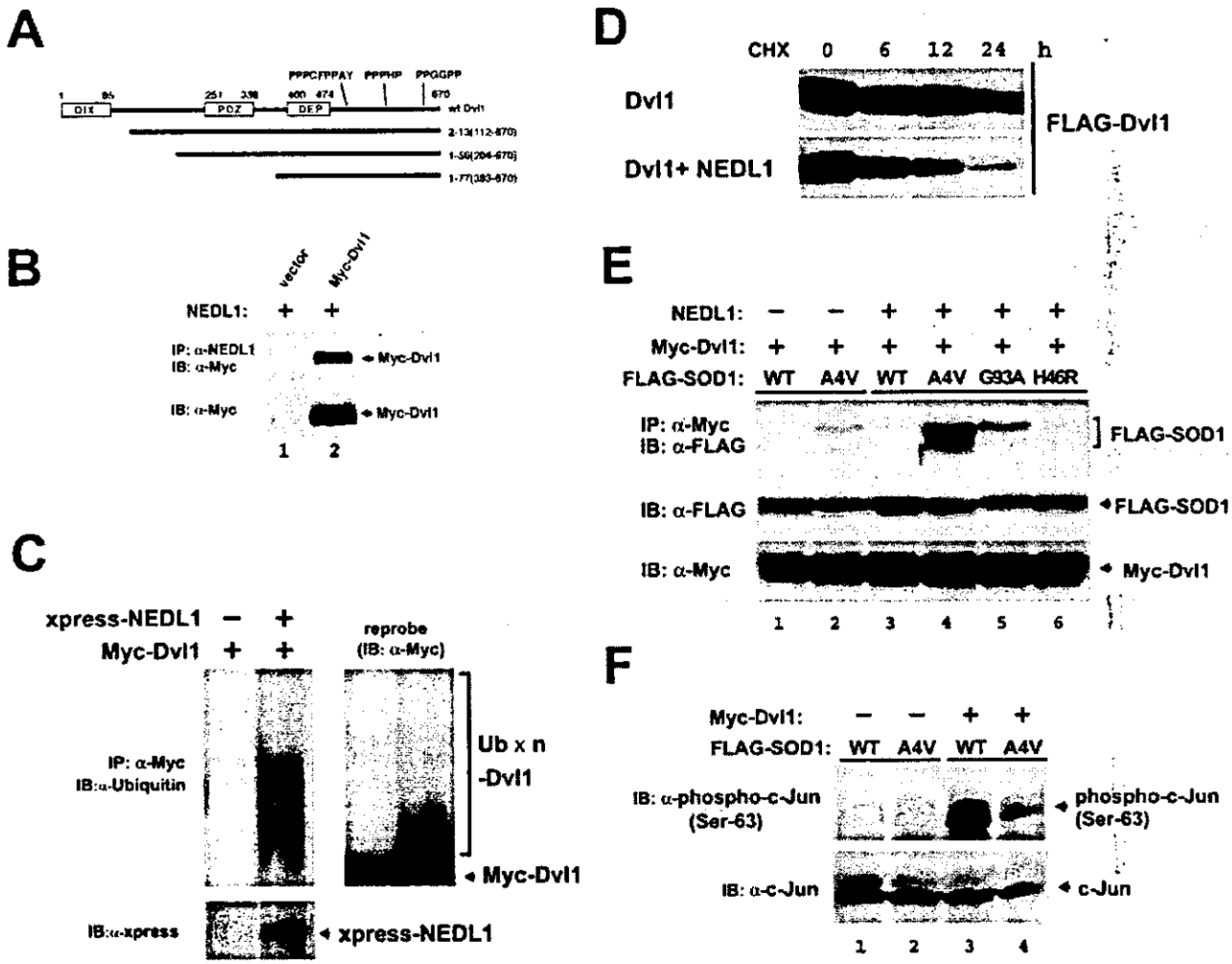

FIG. 6. **Dvl1 is a substrate of NEDL1, and its functions are disturbed by mutant SOD1(A4V).** *A*, schematic illustration of full-length Dvl1 and three clones obtained by yeast two-hybrid screening. Human Dvl1 consists of 670 amino acids and contains three conserved domains, including the DIX, PDZ, and DEP domains. Between the DEP domain and the C-terminal end, there are three proline-rich clusters, which might act as WW domain recognition sites. All three clones (clones 2–13, 1–56, 1–77) contain the DEP domain and these clusters. *B*, NEDL1 interacts with Dvl1. Myc-tagged Dvl1 was overexpressed together with NEDL1 in Neuro2a cells. Whole cell lysates were immunoprecipitated (*IP*) with anti-NEDL1 antibody, followed by immunoblotting (*IB*) with anti-Myc antibody (*upper panel*). The expression levels of Myc-tagged Dvl1 were analyzed by immunoblotting using anti-Myc antibody (*lower panel*). *C*, NEDL1 ubiquitinates Dvl1 in Neuro2a cells. The cells were transiently transfected with the indicated expression plasmids along with the ubiquitin expression plasmid in the presence or absence of the expression plasmid for XPRESS-tagged NEDL1. Whole cell lysates were immunoprecipitated with anti-Myc antibody and then immunoblotted with anti-ubiquitin antibody (*left panel*). The ladder of bands denoted by the *bracket* appeared to be ubiquitinated Dvl1. The expression of XPRESS-NEDL1 was analyzed by immunoblotting using anti-XPRESS antibody. The membrane was reprobed with anti-Myc antibody (*right panel*). *D*, Dvl1 is degraded by NEDL1. Neuro2a cells were transfected with the expression plasmid for FLAG-tagged Dvl1 with or without the NEDL1 expression plasmid. Transfected cells were harvested at different time points as indicated after the addition of cycloheximide (*CHX*; final concentration of 50 μg/ml), and Dvl1 protein levels were analyzed by Western blotting with anti-FLAG antibody. In the presence of NEDL1, the half-lives of FLAG-Dvl1 were significantly reduced. *E*, Dvl1 binds to mutant SOD1(A4V), and the degree of its binding is enhanced in the presence of NEDL1. Whole cell lysates prepared from COS-7 cells transfected with the indicated combinations of expression plasmids were subjected to immunoprecipitation and Western analyses as indicated. *F*, c-Jun phosphorylation by overexpression of Dvl1 is suppressed upon coexpression of mutant SOD1(A4V). Whole cell lysates from COS-7 cells transfected with the indicated combinations of expression plasmids were subjected to Western blotting with antibody against the phosphorylated form of c-Jun (*upper panel*) or with anti-c-Jun antibody (*lower panel*). *wt/WT*, wild-type.

by mutant SOD1. To test this hypothesis, we again performed yeast two-hybrid screening to obtain NEDL1-interacting molecules using the large region of NEDL1 (amino acids 382–1448) as bait. Of 396 His and β-galactosidase double-positive clones, 282 clones were subjected to DNA sequencing, and we identified Dvl1 (three clones). Human Dvl1 is a 670-amino acid protein with three conserved domains: a DIX domain, which is required for canonical Wnt/T-cell factor signaling; a PDZ domain, which is a target of both Stbm and casein kinase I binding; and a DEP domain, which is responsible for Dvl membrane localization during planar cell polarity signaling (25–27). Between the DEP domain and C-terminal end, there are three proline-rich clusters unique to mammalian Dvl1, which presumably act as the WW domain recognition sites. All three clones (clones 2–13, 1–56, and 1–77) contain the DEP domain and proline-rich clusters, suggesting that NEDL1 interacted with Dvl1 in the C-terminal half (Fig. 6*A*). In Neuro2a cells, NEDL1 co-immunoprecipitated with Dvl1 (Fig. 6*B*) and ubiquitinated it for degradation (Fig. 6, *C* and *D*). Thus, Dvl1 may be one of the physiological targets of NEDL1 E3. As recent studies strongly suggest that the cytotoxicity of SOD1 mutants is responsible for their aggregate properties, incorporating other proteins essential for cells into their aggregates (28), we examined the association between mutant SOD1 and Dvl1,

both of which interact with NEDL1. Of interest, Dvl1 bound to mutant SOD1(A4V), and complex formation was increased in the presence of NEDL1 roughly proportionately to the disease severity of FALS caused by the particular SOD1 mutant (Fig. 6*E*). Dvl1 is known to transduce not only the Wnt/β-catenin/T-cell factor pathway, but also the JNK/c-Jun pathway (27). Therefore, we next examined whether the Dvl1-induced phosphorylation of c-Jun at Ser^{63} was affected by the tight complex formation induced by inclusion of mutant SOD1. As shown in Fig. 6*F*, c-Jun phosphorylation induced by overexpression of Dvl1 was significantly suppressed by coexpression with mutant SOD1(A4V) in COS-7 cells.

DISCUSSION

Our present results demonstrate that a novel HECT-type NEDL1 E3, which is preferentially expressed in neuronal tissues, specifically targets mutant forms of SOD1 for ubiquitination-mediated protein degradation. NEDL1 is also associated with TRAP-δ localized at the ER translocon. The TRAP complex has recently been shown to facilitate the initiation of protein translocation in a substrate-specific manner (29). The NEDL1·TRAP-δ complex recognizes mutant (but not wild-type) SOD1, with a binding intensity that broadly parallels the disease severity of FALS. NEDL1 immunoreactivity was detected in the FALS-related LBHIs in the spinal cord ventral horn motor neurons, suggesting that, although mutant SOD1 is ubiquitinated for degradation by NEDL1, the mutant SOD1·NEDL1·TRAP-δ complex aggregates within the LBHIs. It is also conceivable that fragmentation of the Golgi apparatus reported in ALS patients and transgenic mice might be related to this aggregation (30, 31). These findings suggest possible hypotheses for the role of NEDL1 in the pathogenesis of FALS: 1) NEDL1, alone or with TRAP-δ, ubiquitinates and aggregates mutant SOD1, thereby decreasing the function of mutant SOD1; 2) NEDL1 and TRAP-δ form aggregates with mutant SOD1 that induce fragmentation of the Golgi apparatus, leading to neuronal apoptosis; 3) formation of these aggregates causes dysfunction of NEDL1 and/or TRAP-δ, and this, in turn, induces disturbances that ultimately cause motor neuron death; and 4) the mutant SOD1·NEDL1·TRAP-δ aggregates trap and inactivate unknown factor(s) such as molecular chaperones whose normal function is important for motor neuron viability.

To further understand the role of NEDL1 in motor neuron death, we searched for the physiological targets of NEDL1 and identified Dvl1. As expected, Dvl1 is ubiquitinated for degradation by NEDL1. Surprisingly, however, Dvl1 also interacts with mutant SOD1 in the presence of NEDL1 roughly proportionately to the disease severity of FALS caused by the particular SOD1 mutant. Dvl1, an essential multimodule signal transducer localized in the cellular cytosol and cytoskeleton, mediates planar cell polarity signaling as well as canonical Wnt/β-catenin signaling (27, 32). In mammals, three Dvl family members have so far been reported, and the level of Dvl1 expression is high in neuronal tissues (33). As far as we know, NEDL1 is the first E3 for Dvl1, interacting with the C-terminal region containing three proline-rich clusters. A recent report suggests that Dvl1 regulates microtubule stability through inhibition of glycogen synthase kinase-3β (34). Because cytoskeletal abnormalities have been reported in ALS motor neurons (35), it is possible that the effect of mutant SOD1 on NEDL1-mediated Dvl1 degradation is involved in the motor neuron death. Furthermore, Dvl1 is abundant in the postsynaptic membrane region at the neuromuscular junction (36) that is reported to be involved in several neurodegenerative disorders (37, 38). Of interest, *Dvl1* is mapped to chromosome 1p36, which is a commonly deleted region in many human cancers, including neuroblastoma (39). As NEDL1 is highly expressed in neuroblastomas with favorable prognosis, which have a tendency to differentiate and/or regress, NEDL1 may be involved in the regulation of neuronal differentiation and survival possibly by controlling Dvl1.

NEDL1, TRAP-δ, mutant SOD1, and Dvl1 appear to form a complex roughly proportionately to the disease severity of FALS caused by the particular SOD1 mutant. Our present observations strongly suggest that NEDL1 may be a quality control E3 recognizing misfolded mutant SOD1 (40). The association between mutant SOD1 and NEDL1 may induce the conformational change in the NEDL1 protein to increase the binding intensity with other physiological targets such as TRAP-δ (not ubiquitinated) and Dvl1 (ubiquitinated). This may lead to tight complex formation especially when the proteasome activity is impaired. It has been reported that the expression and function of proteasomes decrease with age in the spinal cord (7). Okado-Matsumoto and Fridovich (41) have also found that complex formation between mutant SOD1 and heat shock proteins leads to protein aggregates. Because our data show that the ER translocon component TRAP-δ is involved, aggregate formation may occur at the sites of the ER or Golgi apparatus or even at other cellular sites. The complex formation including NEDL1 and mutant SOD1 may conversely affect the physiological function of NEDL1, as demonstrated by a decrease in Dvl1-induced phosphorylation of c-Jun.

Recently, the RING finger-type E3 Dorfin has been reported to ubiquitinate mutant SOD1 for degradation (42). However, NEDL1 and Dorfin appear to be different in several aspects. First, NEDL1 is expressed specifically in neuronal tissues, including the spinal cord, whereas Dorfin is ubiquitously expressed in most human tissues. Second, both interaction between NEDL1 and mutant SOD1 and ubiquitination of the latter by NEDL1 roughly parallel the disease severity caused by the particular SOD1 mutant, whereas Dorfin similarly ubiquitinates mutant forms of SOD1. In addition, we have identified Dvl1 and TRAP-δ as cellular target proteins of NEDL1, whereas the physiological targets of Dorfin have never been reported. It is probable that there are some other E3 ligases targeting mutant SOD1. However, the molecular characteristics, including tissue-specific expression, subcellular localization, and age-dependent expression, might be important in the development of the FALS phenotype.

In conclusion, we have identified a novel neuronal E3 (NEDL1) that interacts with TRAP-δ and also binds to and ubiquitinates Dvl1 for degradation. Strikingly, NEDL1 targets and ubiquitinates mutant (but not wild-type) SOD1 for degradation. NEDL1 may normally function in the quality control of cellular proteins by eliminating misfolded proteins such as mutant SOD1, possibly via a mechanism analogous to that of ER-associated degradation (43–45). NEDL1 appears to complex tightly with mutant SOD1, Dvl1, and TRAP-δ, forming aggregates with species of mutant SOD1 that have escaped ubiquitin-mediated degradation. The NEDL1 function that affects the activities of the target proteins may also be modulated by mutant SOD1. All of these might contribute to the pathogenesis of FALS; further elucidation of the molecular mechanism of formation of this complex and its pathogenicity may provide insights into motor neuron death in ALS as well as possible new therapeutic strategies for ALS.

Acknowledgments—We thank Robert H. Brown, Jr. (Harvard Medical School) for critical comments and reading the manuscript. We also thank M. Ohira and Y. Nakamura for helping with cDNA cloning and sequencing; K. Watanabe and M. Suzuki for making plasmid constructs; M. Nagai and M. Kato for helping with immunohistochemical studies; S. Hatakeyama, M. Matsumoto, and K. Nakayama